

Bayesian Non-parametric Quantile Process Regression and Estimation of Marginal Quantile Effects

Steven G. Xu¹ and Brian J. Reich¹

Abstract

We propose a non-parametric method to simultaneously estimate non-crossing, non-linear quantile curves. We expand the conditional distribution function of the response in \mathcal{I} -spline basis functions where the coefficients are further modeled as functions of the covariates using feed-forward neural networks. By leveraging the approximation power of splines and neural networks, our model can approximate any continuous quantile function. Compared to existing methods, our method estimates all rather than a finite subset of quantiles, scales well to high dimensions and accounts for estimation uncertainty. While the model is arbitrarily flexible, interpretable marginal quantile effects are estimated using accumulative local effect plots and variable importance measures. A simulation study shows that compared to existing methods, our model can better recover quantiles of the response distribution when the sample size is small, and illustrative applications to birth weight and tropical cyclone intensity are presented.

Key words: Density regression; Hamiltonian Monte Carlo; Interpretable machine learning; Simultaneous quantile estimation.

¹Department of Statistics, North Carolina State University, Raleigh, NC, 27695, USA

1 Introduction

Quantile regression (QR) models the statistical relationship between conditional quantiles of the response distribution and a set of covariates. It allows one to analyze the statistical relationship between covariates and non-central parts of the conditional response distribution. Application of QR has been widely seen in studies where the research question involves modeling the tails of the conditional response distribution. Examples include modeling the 0.05 conditional quantile of birth weight distribution to understand the determining factors of underweight newborns (Abrevaya, 2001) and modeling the 0.99 conditional quantile of wind speed distribution to study the behavior of tropical cyclones that may cause major damage (Elsner et al., 2008).

Modeling a single quantile, however, does not reach the full potential of QR, which lies in the joint description of a set of conditional quantiles. That is, one can model multiple conditional quantiles simultaneously to investigate the functional relationship between covariate effects on the response and quantile level. When used appropriately, multiple QR is a powerful data description tool that offers comprehensive characterization of covariate effects on the conditional response distribution.

However, many QR methods, including the very first proposed by Koenker and Bassett Jr (1978), were designed to estimate quantile-dependent parameters for a single quantile. When these methods are used naively to estimate multiple quantiles, the natural ordering among individually estimated quantiles is not enforced and may lead to estimated quantile curves that cross. That is, for example, the estimated median of the response conditioned on some combination of the covariates might be greater than the estimated 60th percentile. Quantile crossing violates basic probabilistic rules, since any valid conditional quantile function should be monotonically non-decreasing in the quantile level. It can also lead to difficult inference and interpretation, especially when separately estimated quantile curves are used to construct prediction intervals.

Many research works have been proposed to overcome the quantile-crossing problem. Liu and Wu (2009) and Muggeo et al. (2013) proposed to estimate the quantiles sequentially under the constraint that the current quantile curve does not cross the previous one, but their estimation is sensitive to the order that the quantiles are fitted. Chernozhukov et al. (2010) and Rodrigues and Fan

(2017) suggested post-hoc rearrangement of multiple quantile estimates to enforce non-crossing, but the adjusted conditional quantile function still depends highly on the individual estimates which lack strength borrowing across different regression quantiles.

Simultaneous estimation of multiple quantiles has received increasing attention in QR literature. Unlike sequential estimation and post-processing, it estimates all desired quantiles at the same time under non-crossing constraints. Fitting multiple quantiles simultaneously is advantageous since the information used to estimate an individual quantile is shared among estimation of all other quantiles. This can improve overall model performance especially when the available data is sparse. A large literature exists on estimating non-crossing quantile curves simultaneously under a linear regression setting (Bondell et al., 2010; Liu and Wu, 2011; Reich et al., 2011; Reich, 2012; Reich and Smith, 2013; Yuan et al., 2017; Yang and Tokdar, 2017). These approaches enjoy great interpretability by allowing rate-of-change interpretation of quantile-dependent coefficients, but one drawback is that they cannot accommodate non-crossing quantile curves with a complex non-linear trends. Furthermore, they are not suitable for high-dimensional problems since they do not implicitly account for complex interaction effects.

To date, only a few works have considered modeling non-linear quantile curves that do not cross. Cannon (2018) proposed to model the quantile process using a neural network. He treated the quantile level as an additional covariate and imposed partial monotonicity constraints on its associated weight parameters to enforce non-crossing. Although this elegantly alleviates quantile crossing, one consequence is that additional quantile curves for quantile levels not within the specified range have to be estimated via extrapolation. Das and Ghosal (2018) modeled the quantile process as a weighted sum of \mathcal{B} -spline basis functions of the quantile level, where the weights are further expanded by tensor products of \mathcal{B} -spline series expansion of each covariate; order constraints were imposed on the spline coefficients of each covariate to ensure non-crossing. Although their method estimates the whole quantile process, it has a limited model coverage due to the simplified order constraint they chose. Furthermore, tensor product of basis functions is known to not scale well to high dimensions, since the number of parameters grows exponentially with the number of covariates. Non-linear quantile process can also be estimated by inverting (or integrat-

ing then inverting) any valid estimate on the conditional distribution function. Das and Ghosal (2018) proposed a model on the conditional cumulative distribution function (CDF) of similar form to their aforementioned quantile process model. Consequently, their CDF model also suffers from low model coverage and computational intractability in high dimensions. Izbicki and Lee (2016) projected the conditional probability density function (PDF) onto data-dependent eigenfunctions of a kernel-based operator. Their model scales well to high dimensions and also enjoys great model coverage. However, the resulting quantile curves are often not smooth.

In this paper, we propose to simultaneously estimate non-crossing non-linear quantile curves by specifying a Bayesian non-parametric model on the conditional distribution. While there exist other conditional distribution regression models (e.g., Holmes et al., 2012; Rothfuss et al., 2019; Li et al., 2021), we model the conditional CDF using an \mathcal{I} -spline basis expansion where the spline coefficients depend on the covariates through neural networks. We choose to model the distribution function instead of the quantile process because the former permits analytic derivation of the likelihood function and therefore efficient MCMC sampling of the posterior, and for a non-parametric regression the span of potential models is the same in both cases. A spline-based model ensures the estimated conditional CDF, and therefore the estimated conditional quantile function is smooth, and the neural network components allows incorporation of complex covariate effects on the response distribution. A suitable output activation function is chosen for the neural network components such that the model represents a valid CDF. We name this method “QR Using \mathcal{I} -spline Neural Network (QUINN)”. QUINN has a similar form to the density model of Das and Ghosal (2018) but comes with many improvements. Compared to their \mathcal{B} -spline basis expansion, the proposed \mathcal{I} -spline basis expansion reduces the order constraints on the spline coefficients to only a unit simplex constraint. Under this constraint, QUINN can approximate any continuous CDF function. Furthermore, by replacing tensor product of basis functions with neural networks, QUINN enjoys great scalability to high-dimension problems – the growth rate of parameter size is only linear in the number of covariates.

One concern about estimating the quantile process by inverting a non-parametric estimator of the conditional cumulative distribution function is that covariate effects on different quantiles can

be difficult to interpret. In fact, this is a natural drawback for many black box supervised learning models that sacrifice interpretability for flexibility. In many real-world applications, understanding the covariate effects on the predicted response is of paramount importance. In the univariate case, visual characterization of the covariate effect can be obtained by simply plotting the fitted regression line against it. However, black box models such as neural networks are more suitable for multivariate regression problems where an accurate visualization and interpretation of each covariate's main effect is hard to obtain. To overcome this challenge, model-agnostic methods have been developed (Friedman, 2001; Ribeiro et al., 2016; Goldstein et al., 2015) to extract interpretation from black box models. These methods have great advantages over model-specific methods, e.g., the Gini importance for random forest (Breiman, 2001), as they can be applied on any supervised learning method. Recently, Apley and Zhu (2020) proposed to use accumulated local effect (ALE) plots to visualize main and second-order interaction effects of a black box supervised learning model. Their method produces reliable characterization of the covariate effects on the predicted response even if the covariates are correlated. In this paper, we will show that ALE plots can be applied to visualize covariate effects on predicted quantiles. We will also present ways to estimate feature importance of main and second-order interaction effects.

2 Methods

Denote $\mathbf{X} \in \mathcal{X} \subset \mathbb{R}^d$ as the covariate vector and $Y \in \mathbb{R}$ as the scalar response. We are interested in approximating the quantile process of the response given the covariates $Q_Y(\tau|\mathbf{X} = \mathbf{x})$ for quantile level $\tau \in (0, 1)$ and for all $\mathbf{x} \in \mathcal{X}$. If $Q_Y(\tau|\mathbf{x})$ is continuous and monotonically increasing in τ , then for any $\mathbf{x} \in \mathcal{X}$ the conditional CDF is $F_Y(y|\mathbf{x}) = Q_Y^{-1}(\tau|\mathbf{x})$. Thus, the monotonicity constraint of $Q_Y(\tau|\mathbf{x})$ can be naturally accounted for by specifying a valid model on $F_Y(y|\mathbf{x})$ and then inverting it. Our method requires the response variable to have a lower and upper bound. This can be achieved by introducing a transformed response variable $Z = g(Y)$ via a monotonic bijection $g : [L_Y, U_Y] \rightarrow [0, 1]$ where L_Y, U_Y are the bounds of Y ; we consider both finite and infinite values for these bounds. In this section, we will outline our method for approximating quantile process of the transformed response $Q_Z(\tau, \mathbf{x})$ whose estimate can then be back-transformed to an

estimate of $Q_Y(\tau|\mathbf{x})$.

2.1 \mathcal{I} -spline basis expansion

We model the CDF of Z given \mathbf{x} using an \mathcal{I} -spline basis expansion. An \mathcal{I} -spline basis expansion is defined by its support $z \in [L, U]$, degree r and knot sequence $\mathbf{T} = \{t_0, t_1, \dots, t_p | L = t_0 < t_1 \dots < t_p = U\}$. The basis expansion is defined by $r + p - 1$ basis functions $\mathcal{I}_{m,r}(z|\mathbf{T})$ defined as the integral of \mathcal{M} -spline basis functions (Ramsay, 1988) with the same degree and knot sequence

$$\mathcal{I}_{m,r}(z|\mathbf{T}) = \int_L^z \mathcal{M}_{m,r}(u|\mathbf{T}) du.$$

\mathcal{M} -spline basis functions satisfy $\mathcal{M}_{m,r}(z|\mathbf{T}) \geq 0$ and

$$\int_L^U \mathcal{M}_{m,r}(z|\mathbf{T}) dz = 1$$

and thus a convex combination of \mathcal{M} -spline basis functions is a valid probability density function. Also, a non-negative weighted sum of \mathcal{M} -spline basis functions with $r \geq 2$ and uniformly-spaced \mathbf{T} can approximate any non-negative continuous function, with a convergence rate quadratic in the grid size of \mathbf{T} (De Boor and Daniel, 1974). Consequently, a non-negative weighted sum of \mathcal{I} -spline basis functions can approximate any continuous CDF.

2.2 QR using \mathcal{I} -splines and a neural network (QUINN)

Let $F_Z(z|\mathbf{x})$ be the conditional CDF of the transformed response variable Z given \mathbf{x} . A simple but flexible non-parametric model is

$$F_Z(z|\mathbf{x}) = \sum_{m=1}^{r+p-1} \theta_m(\mathbf{x}, \mathcal{W}) \mathcal{I}_{m,r}(z|\mathbf{T})$$

where the spline coefficients $\theta_m(\mathbf{x}, \mathcal{W})$ depend on the covariates \mathbf{x} and parameters \mathcal{W} . The coefficient functions govern the covariate effect on the conditional CDF and therefore should be flexible

enough to capture complex non-linear trends and allow for high-order interaction effects. A modeling framework that comes with these properties is the feed-forward neural network (FNN).

The conditional CDF is valid if and only if the weights $\theta_m(\mathbf{x}, \mathcal{W})$ lie on the simplex. Therefore, we specify the FNN model after a soft-max transformation

$$\theta_m(\mathbf{x}, \mathcal{W}) = \frac{\exp\{u_m(\mathbf{x}, \mathcal{W})\}}{\sum_{i=1}^{r+p-1} \exp\{u_i(\mathbf{x}, \mathcal{W})\}},$$

where the $u_m(\mathbf{x}, \mathcal{W})$ are unconstrained and modeled using a FNN. For simplicity, we describe the FNN with a single hidden layer with V neurons, but extensions to deeper networks are straightforward. The single-hidden-layer FNN model is

$$u_m(\mathbf{x}, \mathcal{W}) = W_{2m0} + \sum_{l=1}^V W_{2ml} \phi \left(W_{1l0} + \sum_{j=1}^d W_{1lj} x_j \right),$$

where $\mathcal{W} = \{W_{uvw}\}$ are the unknown weights and ϕ is the known activation function. Throughout this paper, ϕ is taken to be the hyperbolic tangent function .

The proposed model can approximate any continuous conditional CDF. To see this, define $\{\tilde{\theta}_m(\mathbf{x})\}_{m=1}^{r+p-1}$ as the set of spline coefficients such that $\sum_{m=1}^{r+p-1} \tilde{\theta}_m(\mathbf{x}) \mathcal{I}_{m,r}(z|\mathbf{T})$ approximates $F_Z(z|\mathbf{x})$ arbitrarily well. As described earlier, such a set of coefficients is guaranteed to exist. Then by the universal approximation theorem of the single-hidden-layer FNN, there exist a V and \mathcal{W} so that $\theta_m(\mathbf{x}, \mathcal{W})$ approximates $\tilde{\theta}_m(\mathbf{x})$ arbitrarily well for all m and all $\mathbf{x} \in \mathcal{X}$.

We adopt a Bayesian framework by assigning the prior for the weights \mathcal{W} . Compared to its frequentist counterpart, Bayesian neural network modeling can capture uncertainty in both the fitted model and weight parameters and prior distributions can avoid over-fitting when the sample size is small. For example, putting a Gaussian prior on the weights is equivalent to imposing a \mathcal{L}_2 -penalty on their magnitudes. For priors, we select $W_{1vw} \stackrel{\text{indep}}{\sim} \mathcal{N}(0, \sigma_w^2)$, $W_{2vw} \stackrel{\text{indep}}{\sim} \mathcal{N}(0, \gamma^2)$ and $\sigma_w, \gamma \stackrel{\text{iid}}{\sim} \mathcal{N}^+(0, a^2)$, where the scale parameters are distributed according to the Half-Gaussian distribution with scale parameter a . Appendix A describes the Hamiltonian Monte Carlo algorithm used to approximate the posterior and code is available at <https://github.com/stevennxu/quinn>.

Our ultimate goal is to estimate the quantile process of the original response variable $Q_Y(\tau|\mathbf{x})$.

Let $\hat{F}_Z(z|\mathbf{x})$ denote the conditional CDF estimator and $\mathbf{D}_Z = \{\tilde{z}_1, \tilde{z}_2, \dots, \tilde{z}_N\}$ denote a dense grid on the unit interval. Non-parametric estimate of the quantile process $Q_Z(\tau|\mathbf{x})$ can be easily obtained by first evaluating $\hat{F}_Z(z|\mathbf{x})$ on \mathbf{D}_Z and then performing linear interpolation on a dense percentile grid by treating $\{\hat{F}_Z(z_i|\mathbf{x})\}_{i=1}^N$ as the input values and \mathbf{D}_Z as the functional output values. Because of the one-to-one correspondence between quantile function and CDF, the resulting quantile process estimator will also inherit the approximator property of the proposed CDF estimator. Finally, the estimated quantile process of the original response is given by $\hat{Q}_Y(\tau|\mathbf{x}) = g^{-1} [\hat{Q}_Z(\tau|\mathbf{x})]$.

3 Summarizing covariate effects

As described in Section 2, QUINN includes a flexible FNN model for covariate effects across quantile levels. FNN is a “black box” supervised learning model that provides abundance of flexibility but suffers from lack of transparency and accountability. Unlike linear QR models which enable rate-of-change interpretation of the τ -dependent coefficients, the proposed FNN-based model does not inherently explain the covariate effects on the predicted quantile in an understandable way. This is a considerable drawback, especially since QR models are more often used for explanatory purposes (e.g., identifying trends in the change of conditional quantiles when varying a covariate).

Fortunately, the explosion of work on model agnostic tools in the last two decades has included numerous methods to visualize and understand main effects of individual covariates, and even second-order interaction effects between pairs of covariates (we omit consideration of higher order effects as they cannot be visualized or interpreted meaningfully) on the predictions made by “black box” models. The most famous model agnostic tool is partial dependence plot (PD plot) which visualizes the average marginal effect a (pair of) covariate(s) have on the predictions. The PD plot is straightforward to implement and intuitive to interpret, but its assumption of covariate independence renders it unreliable when a subset of covariates are strongly correlated. Apley and Zhu (2020) proposed accumulative local effects (ALEs) plot that not only avoids the collinearity problem of the PD plot but also provides the same level of interpretation in a faster way. In this section, we provide a brief review of the definitions of ALE plot and explain how it can be extended

to QR models. We will later demonstrate using a multivariate simulation study how ALE plot can be used to visualize and understand covariate effects of QUINN.

The sensitivity of $Q_Y(\tau|\mathbf{x})$ to covariate j is naturally quantified by the derivative $q_j(\tau, \mathbf{x}) = \partial Q_Y(\tau|\mathbf{x})/\partial x_j$. In a linear QR, the derivative is the scalar effect of covariate j on quantile level τ , but for a non-linear regression function the derivative depends on \mathbf{x} . The ALE begins by averaging $q_j(\tau, \mathbf{X})$ over \mathbf{X} conditioned on $X_j = x_j$, giving $\bar{q}_j(\tau, x_j) = \mathbb{E}_{\mathbf{X}} [q_j(\tau, \mathbf{X})|X_j = x_j]$. The uncentered ALE main effect function of X_j is then defined as

$$\bar{Q}_j^U(\tau, x_j) = \int_{x_{\min,j}}^{x_j} \bar{q}_j(\tau, u_j) du_j.$$

The function $\bar{Q}_j^U(\tau, x_j)$ can be interpreted as the ALE of X_j in the sense that it is an accumulation of local effects $\bar{q}_j(\tau, u_j)$ averaged over the distribution of \mathbf{X} . The uncentered ALE effect does not have a straightforward interpretation because the derivative is invariant to scalar addition, which leads to the definition of the (centered) ALE main effect function $\bar{Q}_j(\tau, x_j)$ that is the same as $\bar{Q}_j^U(\tau, x_j)$ except centered to have mean 0 with respect to the marginal distribution of X_j .

Analogous formulas define the second-order ALE for X_j and X_l . Consider the second-order partial derivative $q_{jl}(\tau, \mathbf{x}) = \partial^2 Q_Y(\tau|\mathbf{x})/\partial x_j \partial x_l$. The local effect at $X_j = x_j$ and $X_l = x_l$, averaging over the other covariates, is $\bar{q}_{jl}(\tau, x_j, x_l) = \mathbb{E}_{\mathbf{X}} [q_{jl}(\tau, \mathbf{X})|X_j = x_j, X_l = x_l]$. The uncentered second-order ALE is then

$$\bar{Q}_{jl}^U(\tau, x_j, x_l) = \int_{x_{\min,j}}^{x_j} \int_{x_{\min,l}}^{x_l} \bar{q}_{jl}(\tau, u_j, u_l) du_j du_l,$$

and the second-order ALE function $\bar{Q}_{jl}(\tau, x_j, x_l)$ is mean-centered with respect to the marginal distribution of (X_j, X_l) . The second-order ALE $\bar{Q}_{jl}(\tau, x_j, x_l)$ describes the joint effects of the two covariates, which consist of both their main effects and interaction effect. In cases where assessment of the interaction effect is of interest, $\bar{Q}_{jl}(\tau, x_j, x_l)$ can be further centered with respect to the main effects of X_j and X_l to obtain the pure interaction effect $\bar{Q}_{jl}^I(\tau, x_j, x_l)$, i.e., $\bar{Q}_{jl}^I(\tau, x_j, x_l) = \bar{Q}_{jl}(\tau, x_j, x_l) - \bar{Q}_j(\tau, x_j) - \bar{Q}_l(\tau, x_l)$.

The functions $\bar{Q}_j(\tau, x_j)$, $\bar{Q}_{jl}(\tau, x_j, x_l)$, and $\bar{Q}_{jl}^I(\tau, x_j, x_l)$ can be plotted to understand each

main and (second-order) interaction effect. When plotted against x_j , the main ALE $\bar{Q}_j(\tau, x_j)$ quantifies the difference between average prediction conditioned on $X_j = x_j$ and the average prediction over \mathbf{X} . For example, $\bar{Q}_j(\tau, 1) = -5$ means that $\mathbb{E}_{\mathbf{X}}[Q(\tau, \mathbf{X}|X_2 = 1)] = \mathbb{E}_{\mathbf{X}}[Q(\tau, \mathbf{X})] - 5$. When plotted against x_j and x_l , the second-order ALE $\bar{Q}_{jl}(\tau, x_j, x_l)$ quantifies the difference between average prediction conditioned on $(X_j, X_l) = (x_j, x_l)$ and the average prediction over \mathbf{X} . For example, $\bar{Q}_{1,3}(\tau, -1, 1) = 2$ means that $\mathbb{E}_{\mathbf{X}}[Q(\tau, \mathbf{X}|X_1 = -1, X_3 = 1)] = \mathbb{E}_{\mathbf{X}}[Q(\tau, \mathbf{X})] + 2$. The interaction ALE $\bar{Q}_{jl}^I(\tau, x_j, x_l)$ can be interpreted analogously to $\bar{Q}_{jl}(\tau, x_j, x_l)$, except now the difference is contributed entirely by the interaction effect.

It is also useful to summarize the main and interaction ALEs with a one-number summary that can be used to rank the importance of each effect. Following Greenwell et al. (2018), we propose to measure overall variable importance (VI) for continuous covariates using the standard deviation of the ALE with respect to the marginal distribution of \mathbf{X} , i.e.,

$$\text{VI}_j(\tau) = \text{SD}[\bar{Q}_j(\tau, X_j)] \quad \text{and} \quad \text{VI}_{jl}(\tau) = \text{SD}[\bar{Q}_{jl}^I(\tau, X_j, X_l)];$$

for categorical covariates, the standard deviation is replaced by one fourth of the range. These VI scores (and the intermediate functions \bar{Q}_j , \bar{Q}_{jl} , and \bar{Q}_{jl}^I) can be approximated using the partitioning schemes of Apley and Zhu (2020) as described in Appendix B.

Although for notational simplicity we have omitted the dependence of the quantile function on the parameters \mathcal{W} , in practice the posterior uncertainty in \mathcal{W} leads to posterior uncertainty in the sensitivity metrics such as $\bar{Q}_j(\tau)$ and $\text{VI}_j(\tau)$. We account for this uncertainty by computing the sensitivity measures for many MCMC samples from the posterior distribution of \mathcal{W} , giving a Monte Carlo approximation of the posterior distribution of the sensitivity measures.

4 Simulation

4.1 Univariate and bivariate \mathbf{X}

We first investigate performance for three cases with univariate and bivariate \mathbf{X} :

Design 1. The covariate X is generated from $\mathcal{U}(0, 5)$. The response variable Y is given by

$$Y = X + \sin(2X) + 3\epsilon,$$

where ϵ follows the skew-normal distribution with location parameter 0, scale parameter 1 and shape parameter 4. The resulting quantile curves are parallel, and the data is highly right-skewed.

Design 2. The covariate X is generated from $\mathcal{U}(0, 1)$. The response variable Y is given by

$$Y = 3X + [0.5 + 2X + \sin(3\pi X + 1)]\epsilon,$$

where ϵ follows the normal distribution with mean 0 and standard deviation 1. The resulting quantile curves are linear at the median but have strong curvature at the extremes.

Design 3. The covariate vector $\mathbf{X} = (X_1, X_2)$ is generated from $\mathcal{U}(0, 1) \times \mathcal{U}(0, 1)$. The response variable Y is given by

$$Y = \sin(2\pi X_1) + \cos(2\pi X_2) + \sqrt{2(X_1^2 + X_2^2)}\epsilon,$$

where ϵ follows \mathcal{T}_3 , the Student's t distribution with three degrees of freedom. The data exhibit strong heteroscedasticity and heavy-tailedness. For each design, we generate sample of sizes $n \in \{50, 100, 200\}$. Quantile curves (surfaces) at nineteen equally spaced quantiles $\tau \in \{0.05, 0.10, \dots, 0.95\}$ are fitted to the data.

To assess the performance of the proposed method in recovering non-linear quantile process from simulated data, we compare our method to four non-parametric non-crossing QR methods: the monotone composite QR neural network (MCQRNN) of Cannon (2018), the non-parametric simultaneous QR (NPSQR) of Das and Ghosal (2018), the non-parametric distribution function simultaneous QR (NPDFSQR) also of Das and Ghosal (2018), and the spectral series conditional density estimator (seriesCDE) of Izbicki and Lee (2016). MCQRNN is implemented in the `qrnn` package in R; codes for NPSQR and NPDFSQR are available from the second author's webpage; and codes for seriesCDE are available from the supplemental material of the online paper. Implementation details including tuning and model selection are given in Appendix C. For QUINN, we

run NUTS for 2000 iterations and discard the first 1000 iterations as burn-in.

To compare the methods, 100 data sets were simulated for each design. For each sample size, the overall performance of each method is measured by the root mean integrated square error (RMISE) between the actual, $Q_Y(\tau|\mathbf{x})$, and estimated (posterior mean), $\hat{Q}_Y(\tau|\mathbf{x})$, quantile processes. To calculate the RMISE, we first divide the domain of each dimension of \mathbf{X} by g equidistant grid-points, giving the $G = gd$ vectors $\tilde{\mathbf{x}}_1, \dots, \tilde{\mathbf{x}}_G$ that span the range of \mathbf{X} . For Designs 1 and 2, we set $g = G = 101$ and for Design 3 we set $g = 41$ and thus $G = 41^2$. The RMISE is then approximated as

$$\text{RMISE}(\tau_k) = \sqrt{\frac{1}{G} \sum_{i=1}^G \left\{ Q_Y(\tau_k|\tilde{\mathbf{x}}_i) - \hat{Q}(\tau_k, \tilde{\mathbf{x}}_i) \right\}^2}$$

for quantile level $\tau_k \in \{0.05, 0.10, \dots, 0.95\}$ and

$$\text{RMISE}_{\text{QP}} = \sqrt{\frac{1}{19} \sum_{k=1}^{19} \text{RMISE}(\tau_k)^2}$$

for the entire quantile process.

The average RMISE_{QP} over 100 simulated data sets for each method, along with their standard errors, are shown in Table 1. We see that for each of the designs considered, QUINN and MCQRNN give the best estimation. Specifically, QUINN gives significantly better estimation when the sample size is small, whereas the performance of MCQRNN catches up when the sample size becomes large. QUINN also results in a more robust fit when data is scarce, in contrast to MCQRNN which has a drastically high variance. The only case where MCQRNN significantly outperformed QUINN is Design 3 with $n = 200$. This is expected, as the min-max normalization is not a bijection between $[U_Y, Y_L]$ and $[0, 1]$ when Y is unbounded and results in only a truncated $F_Y(y|\mathbf{x})$ being estimated for all \mathbf{x} . This truncation will acutely impact estimate of extreme quantiles of a heavy-tailed distribution like \mathcal{T}_3 in a finite sample setting. Nonetheless, QUINN still achieves similar and even better performance than existing methods when the sample size is small. The average $\text{RMISE}(\tau)$ for each method over 100 simulated data sets are shown in Figure 1. We

Table 1: **Simulation results:** Average RMISE_{QP} over 100 simulated data sets with standard error in parentheses, and the smallest error in each row is in bold.

Design	n	QUINN	MCQRNN	NPSQR	NPDFSQR	seriesCDE
1	50	0.89 (0.26)	1.11 (1.98)	1.13 (0.26)	1.15 (0.26)	1.11 (0.29)
	100	0.62 (0.11)	0.65 (0.15)	1.00 (0.19)	0.89 (0.17)	0.87 (0.19)
	200	0.49 (0.09)	0.47 (0.11)	0.96 (0.18)	0.74 (0.16)	0.71 (0.19)
2	50	0.80 (0.16)	1.18 (2.28)	1.18 (0.28)	1.20 (0.31)	0.90 (0.20)
	100	0.60 (0.11)	0.72 (0.13)	1.19 (0.22)	0.93 (0.19)	0.74 (0.19)
	200	0.47 (0.07)	0.53 (0.11)	1.03 (0.18)	0.76 (0.15)	0.57 (0.15)
3	50	1.19 (0.32)	1.39 (0.81)	2.23 (1.78)	2.68 (2.25)	1.23 (0.53)
	100	0.94 (0.26)	0.94 (0.21)	2.33 (1.83)	4.04 (2.62)	0.96 (0.27)
	200	0.81 (0.31)	0.71 (0.34)	2.16 (1.20)	3.66 (2.29)	0.86 (0.27)
4	200	2.58 (0.27)	3.21 (1.58)	-	-	3.37 (0.21)

see that QUINN gives the best estimation of nonextreme quantiles in all cases, whereas MCQRNN gives similar or even better estimation of extreme quantiles when the data exhibit significant heavy-tailedness or skewness.

4.2 Multivariate \mathbf{X}

A defining characteristic of a non-parametric regression model is its ability to account for complex interaction effects. Similarly, non-parametric QR model accounts for quantile-dependent interaction effects. Therefore, we would like to assess the performance of QUINN when \mathbf{X} is multivariate and has both quantile-independant and quantile-dependent interaction effects. In addition, we would like to assess the performance of QUINN when the data have a sparse structure; i.e., only a subset of given covariates actually influences the response. To address these questions, we consider a ten-predictor simulation design:

Design 4. The covariate vector $\mathbf{X} = (X_1, X_2, \dots, X_{10})$ is generated uniformly from $[0, 1]^{10}$. The

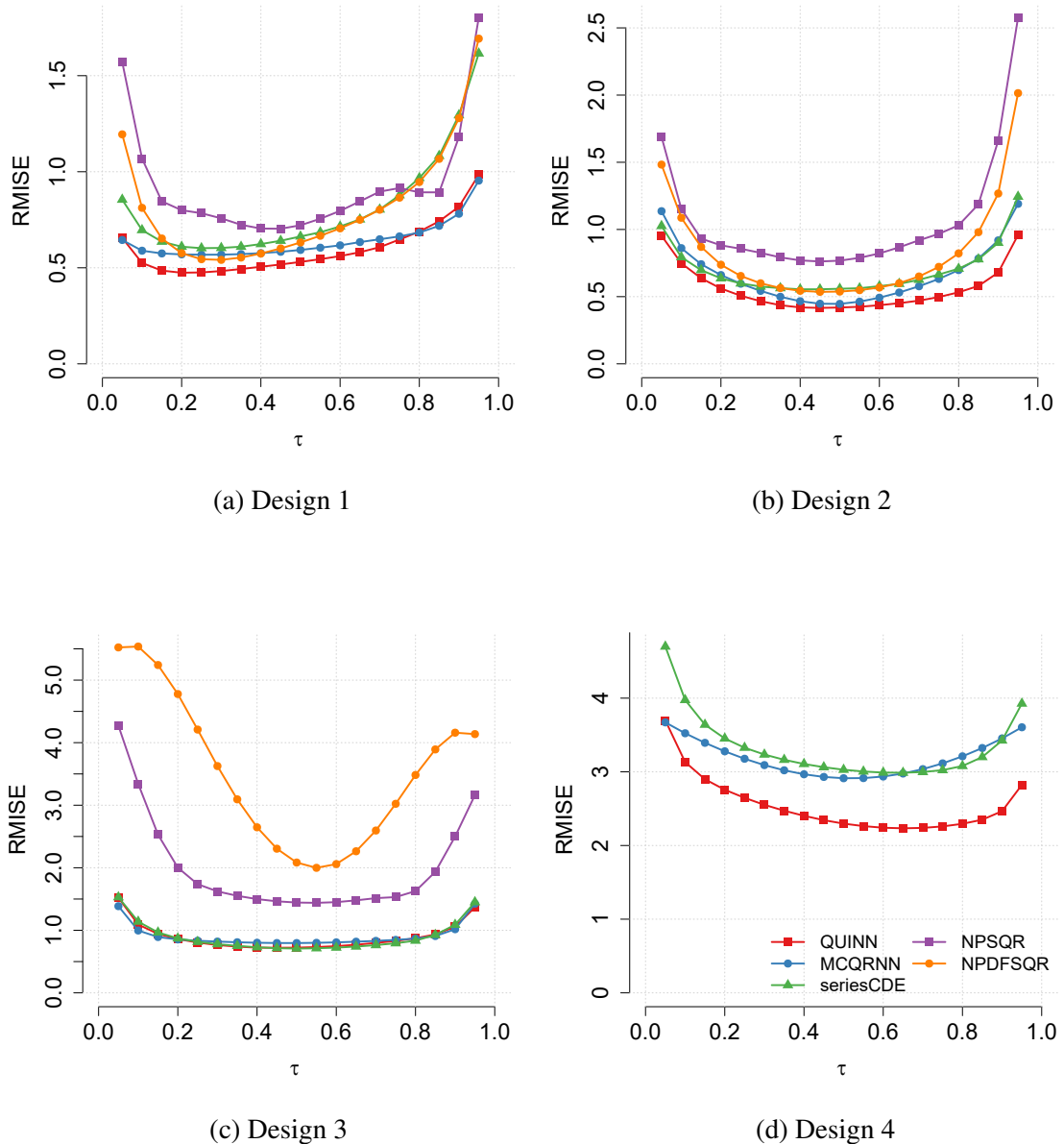


Figure 1: **Simulation results by quantile level.** Average RMISE(τ) over 100 simulated data sets by quantile level τ .

quantile function of the response variable conditioned on the covariate $Q_Y(\tau|\mathbf{x})$ is given by

$$\begin{aligned} Q_Y(\tau|\mathbf{x}) = & 3(\tau - 0.5) \left(X_1 + \frac{3}{5} \right)^3 + 15 \left[X_2 + 4 \left(X_2 - \frac{1}{2} \right)^2 \right] \exp(-X_2^2) \\ & + 12 \exp \left[\left(X_3 + \frac{1}{2} \right)^2 \left(X_4 - \frac{1}{2} \right)^2 \right] + 5(\tau - 1) \left(X_5 + \frac{2}{5} \right) \left(X_6 + \frac{1}{2} \right)^2, \\ & + 0.25\Phi^{-1}(\tau) \end{aligned}$$

where $\Phi^{-1}(\cdot)$ is the standard normal quantile function. In this design, X_3 and X_4 have a quantile-independent interaction effect, and X_5 and X_6 have a quantile-dependent interaction effect. The design is sparse as only the first six covariates are relevant.

For the multivariate design, we compare QUINN with MCQRNN and seriesCDE only. We omit NPSQR and NPDFSQR because expanding each covariate of a d -dimensional \mathbf{x} using quadratic \mathcal{B} -spline basis functions results in a parameter space of dimension $p_{\text{DG}}(p_{\text{DG}} + 2)^d$. That is, the number of parameters in NPSQR and NPDFSQR grow exponentially with the number of covariates. Even with d as few as 10, fitting NPSQR and NPDFSQR becomes computationally infeasible. We generate sample of size $n = 400$ and split into 200 training and 200 testing data points. Each model is first fit to the training data, then conditional quantile predictions at the equally-spaced quantiles mentioned in Section 4.1 are calculated for each given \mathbf{x} of the testing data. For QUINN, we run NUTS for 3500 iterations and discard the first 2500 iterations as burn-ins.

To measure the performance of each method, we generate 100 data sets; and for each data set we calculate RMISE_τ between actual and predicted quantiles conditioned on the testing data points. The average RMISE_τ over 100 simulated data sets are shown in Figure 1(d). We see that QUINN gives substantially better estimation of the quantile process than MCQRNN and seriesCDE. The result shows that our proposed method maintains its promising performance when \mathbf{x} is multivariate, has complex interaction effects, and has a sparse structure.

We now demonstrate how ALEs plot can be used with QUINN to visualize main and second-order interaction effects on its predicted quantiles. Design 4 is constructed such that only $\bar{Q}_1(\tau, x_1)$, ..., $\bar{Q}_6(\tau, x_6)$, $\bar{Q}_{34}(\tau, x_3, x_4)$, and $\bar{Q}_{56}(\tau, x_5, x_6)$ are non-zero for some or all τ . In addition,

$\bar{Q}_j(\tau, x_j)$, $j = 1, 5, 6$ and $\bar{Q}_{56}(\tau, x_5, x_6)$ vary across τ . For each of the 100 simulated data sets, we calculate the ALE main effect for each covariate and interaction effect for each pair of covariates at quantile levels $\tau \in \{0.05, 0.10, \dots, 0.95\}$. The estimated ALE main effects at quantile levels $\tau \in \{0.05, 0.50, 0.95\}$ are shown in Figure 2; where the gray lines represent individual estimates based on the 100 simulated data sets, and the red line represents the true ALE effect calculated using the generating model. The estimated ALEs precisely capture the quantile-independent main effects of X_2, X_3, X_4 , the quantile-dependent main effects of X_1, X_5, X_6 , and the redundancy of X_7, X_8, X_9, X_{10} . We also compare VI scores calculated from the estimated effects to those from the true effects in Figure 3. The ranking of the covariates based on estimated VI scores resembles that based on true VI scores.

The estimated interaction effects are analyzed in Figure 4, where the off-diagonal cells contain VI scores of pair-wise interaction effects. Our results show that when $\tau = 0.05$ or 0.50 , the estimated VI scores of $\bar{Q}_{34}(\tau, x_3, x_4)$ and $\bar{Q}_{56}(\tau, x_5, x_6)$, the only two interaction effects that contribute to the generating model, are significantly higher than those of all other pairs; when $\tau = 0.95$, $\bar{Q}_{56}(\tau, x_5, x_6)$ is close to zero and thus was difficult to distinguish from other non-contributing interaction effects. We further calculate the Monte Carlo probability that $\bar{Q}_{34}(\tau, x_3, x_4)$ or $\bar{Q}_{56}(\tau, x_5, x_6)$ is ranked top 2 among all interaction effects and show the results in Figure 5. The probability that $\bar{Q}_{34}(\tau, x_3, x_4)$ is ranked top 2 is close to 1 across all quantiles; the probability that $\bar{Q}_{56}(\tau, x_5, x_6)$ is ranked top 2 is close to 1 when $\tau < 0.6$, but decreases as $\bar{Q}_{56}(\tau, x_5, x_6)$ decreases. Therefore, the sensitivity analysis consistently identified the important main and interaction effects.

5 Applications

5.1 Application to cyclone intensity data

Elsner et al. (2008) argued that the strongest tropical cyclones in the North Atlantic Basin have gotten stronger recently as a result of increasing ocean temperature over the Atlantic Ocean. They analyzed 291 tropical cyclones over the period 1981 – 2006 and used separate QRs to model the relationship between their satellite-derived lifetime-maximum wind speed (W_{maxST}) and year of

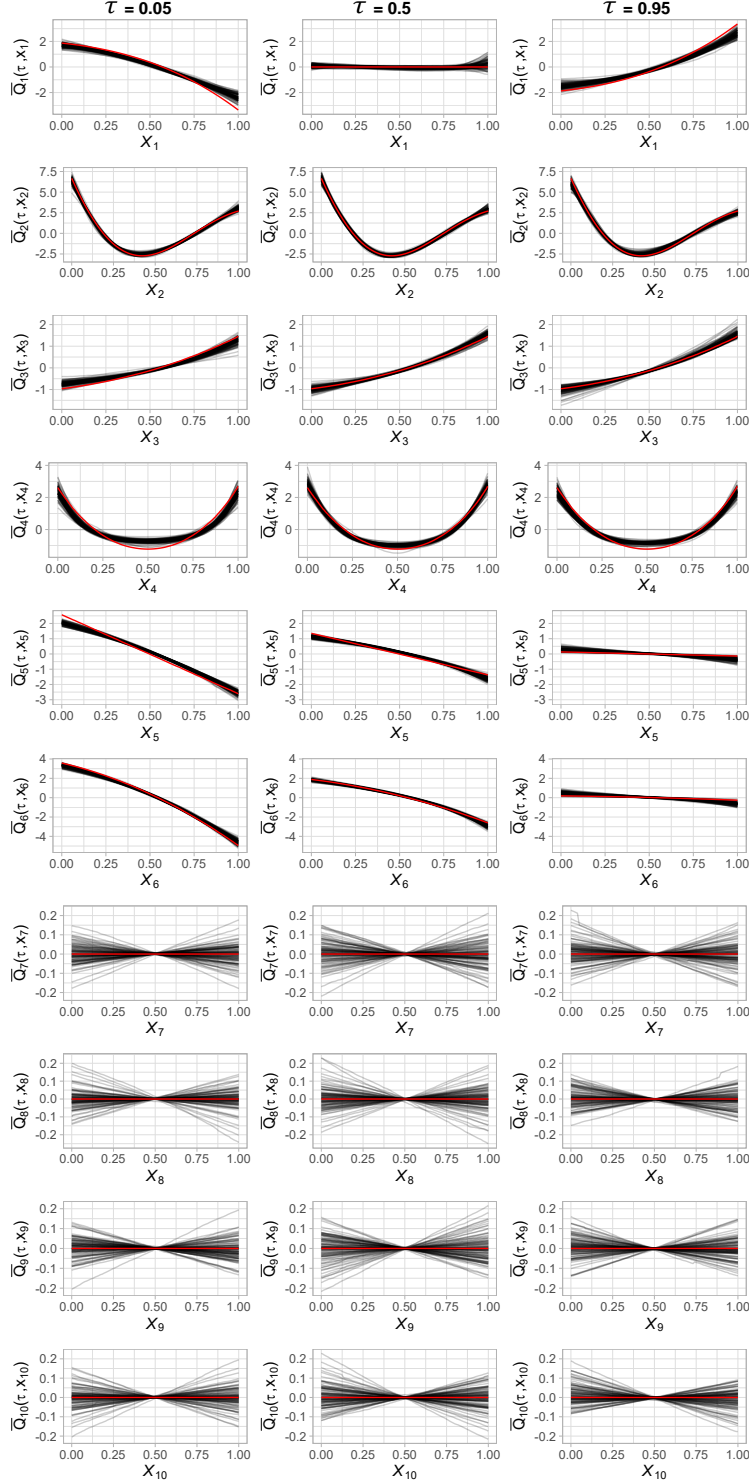
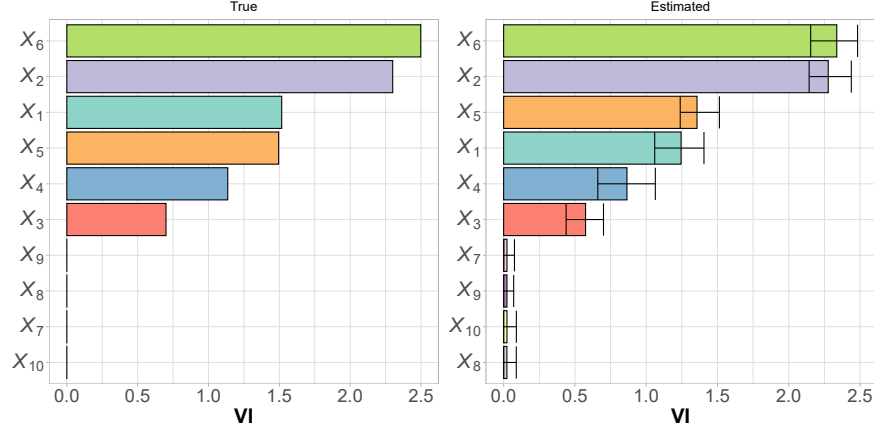
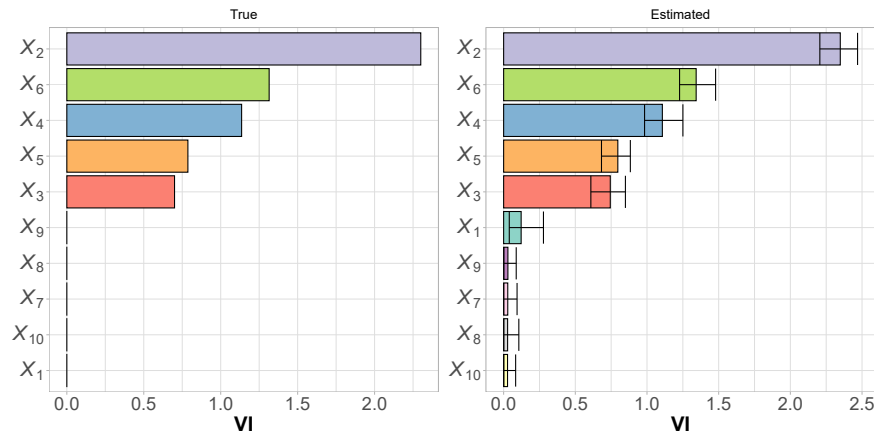


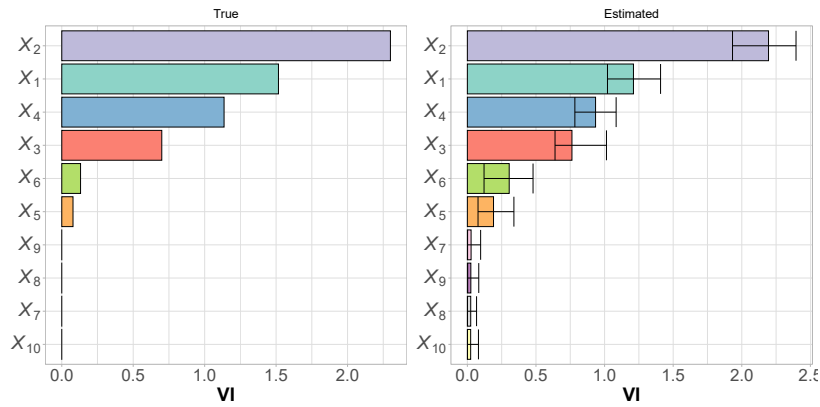
Figure 2: **Marginal main effect estimates for Simulation Design 4.** Accumulative local effects (ALE) $\bar{Q}_j(\tau)$ by covariate $j \in \{1, \dots, 10\}$ and quantile level $\tau \in \{0.05, 0.50, 0.95\}$. The gray lines represent individual ALE calculated from the 100 simulated data sets. The red line represents the true ALE calculated from the generating model.



(a) Quantile level $\tau = 0.05$

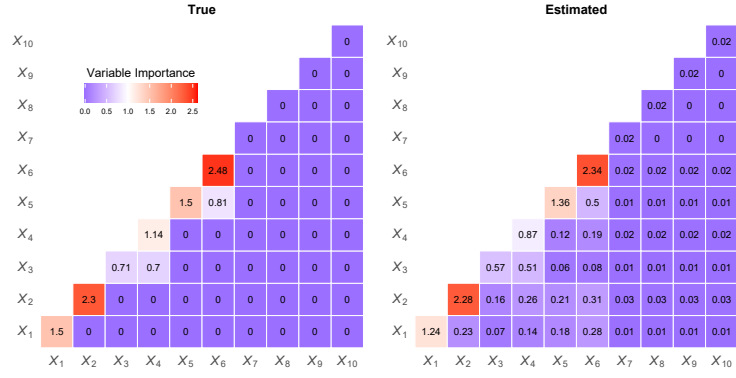


(b) Quantile level $\tau = 0.50$

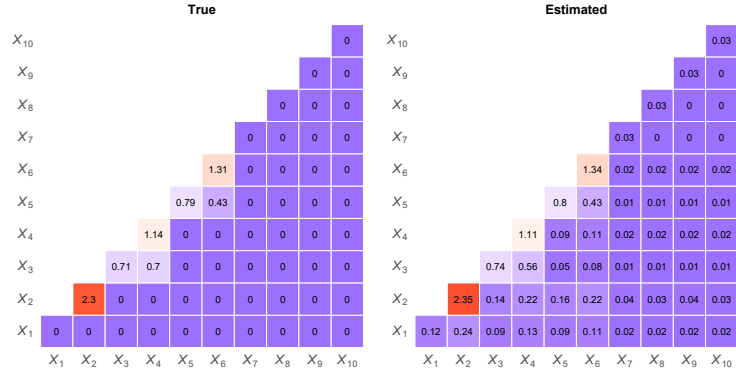


(c) Quantile level $\tau = 0.95$

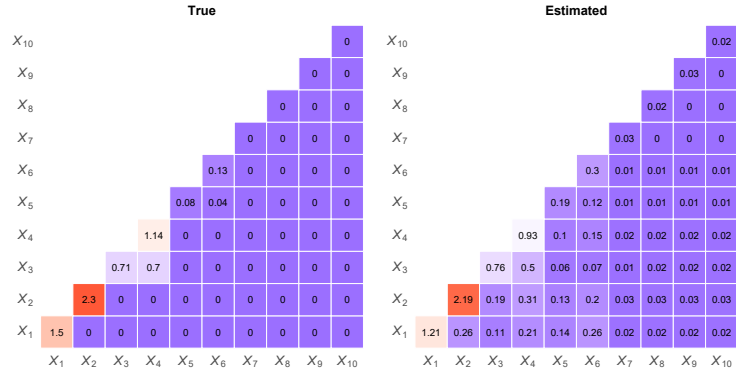
Figure 3: **Marginal main effects importance for Simulation Design 4.** Average estimated (left) and true (right) variable importance $VI_j(\tau)$ for each main effect and $\tau \in \{0.05, 0.50, 0.95\}$; the estimates are averaged over 100 datasets and thin horizontal lines are 95% intervals.



(a) Quantile level $\tau = 0.05$



(b) Quantile level $\tau = 0.50$



(c) Quantile level $\tau = 0.95$

Figure 4: **Marginal interaction effects importance for Simulation Design 4.** Average estimated (left) and true (right) variable importance $VI_{jk}(\tau)$ for each interaction effect; the estimates are averaged over 100 datasets.

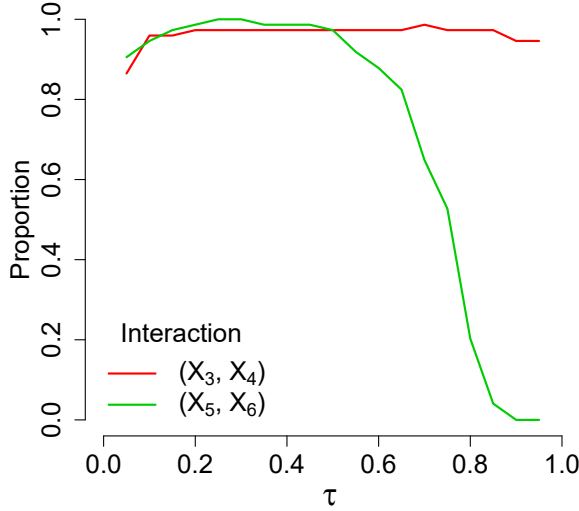


Figure 5: **Marginal interaction effects importance ranking for Simulation Design 4.** Proportion of the 100 simulated datasets for which the variable importance of $\bar{Q}_{jl}^I(\tau, X_3, X_4)$ and $\bar{Q}_{jl}^I(\tau, X_5, X_6)$ are ranked top 2 among all second-order interaction effects.

occurrence (`Year`) over a set of quantile levels. They found significant upward trends for regression lines modeling quantile levels above the 70th percentile ($\tau > 0.7$) with estimated slope coefficient increasing with τ . One drawback of their analysis was that they did not consider non-linear QR. In this section, we present an analysis of the data provided by Elsner et al. (2008) and model the wind speed quantiles simultaneously and non-parametrically using QUINN.

First, we transform the covariate `Year` linearly to the unit interval such that the years 1981 and 2006 are mapped to 0 and 1 respectively. For the response variable `WmaxST`, we considered three transformations to the unit interval: min-max normalization, log transformation followed by min-max normalization, and CDF transformation using the power-Pareto distribution given by

$$F(y) = 1 - \frac{1}{(1 + (y/\sigma)^k)^a},$$

where $a = 0.45$, $\sigma = 52$ and $k = 4.9$ (Tokdar et al., 2012; Das and Ghosal, 2018). We fit QUINN with $V \in \{5, 8, 10, 15\}$ hidden neurons and $p \in \{5, 8, 10, 12\}$ spline knots. We draw 2000 posterior samples using NUTS, disregarding the first 1000 samples as burn-in and choose the

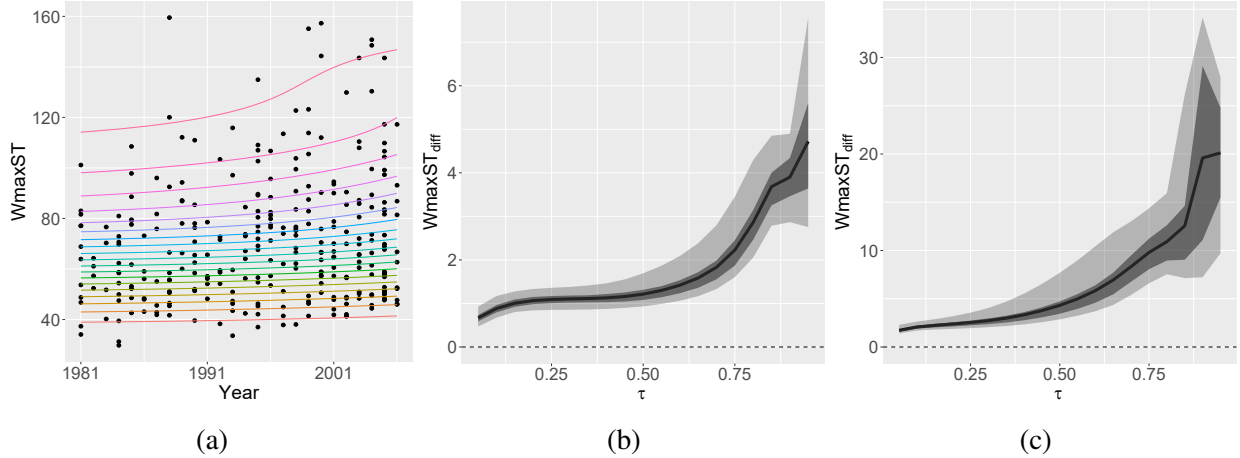


Figure 6: Cyclone intensity analysis. (a) Scatter plot of satellite-derived lifetime-maximum wind speed ($W_{\max ST}$) and year of occurrence ($Year$) overlaid with quantile curves estimated by QUINN. (b) Posterior mean difference (solid black line) of $W_{\max ST}$ between year 1990 and 1981 across quantile range $\tau \in [0.05, 0.95]$ with 50% (light grey region) and 95% (dark grey region) credible band. (c) Posterior mean difference (solid black line) of $W_{\max ST}$ quantiles between year 2006 and 1997 across $\tau \in [0.05, 0.95]$ with 50% (light grey region) and 95% (dark grey region) credible bands.

best configuration of transformation method, V and p based on WAIC of the fitted model.

The scatter plot of the cyclone intensity data is shown in Figure 6 where each point represents a tropical cyclone between 1981 and 2006. The plot is overlaid with quantile curves for $\tau \in \{0.05, 0.10, \dots, 0.95\}$ estimated by QUINN. We observe that all quantile curves are smooth, showing monotonically increasing trends over τ . Furthermore, the increase is more significant in recent years and at higher quantile levels. This shows that tropical cyclones are getting stronger from 1980 to 2007, with the strongest ones having the most significant increase. We also visualize the posterior estimates of the change in $W_{\max ST}$ quantiles between 1981 and 1990, and between 1997 and 2006 in Figure 6, i.e., $W_{\max ST_{\text{diff}}} = Q_Y(\tau|x_2) - Q_Y(\tau|x_1)$ where x_1 and x_2 are the transformed covariates for the two years in the comparison. We see that in both cases the posterior mean $W_{\max ST_{\text{diff}}}$ increases as τ increases, and the magnitude of $W_{\max ST_{\text{diff}}}$ quantiles between 1997 and 2006 is greater than that between 1981 and 1990, supporting our previous observations. Furthermore, the 95% credible intervals are above 0, showing that the increase of intensity for cyclones between 1980 and 2007 is statistically significant.

5.2 Application to birth weight data

For the case of multivariate data analysis, we present an analysis of the effect of pregnancy-related factors on infant birth weight (`Weight`, in grams) quantiles. This effect was first studied in detail using separate linear regression and 1992 and 1996 editions of the Natality Data Set (Abrevaya, 2001); it was then restudied using simultaneous linear QR and 1997 edition of the data set (Tokdar et al., 2012). In this paper, we consider birth records from a more recent edition and present inference result from estimating the effect non-parametrically using QUINN. Our data consist of 5000 randomly chosen entries from the 2019 edition of the Natality Data Set of the United States² on singleton live births to mothers recorded as Black or White, in the age group 18–45, with height between 59 and 73 inches, and smoke no more than 20 cigarettes daily during pregnancy. The list of covariates includes gender of the child (`Boy`, 1 = boy, 0 = girl), length of gestation (`Week`), maternal age (`Age`, in years), race (`Black`, 1 = Black, 0 = White), height (`Height`, in inches), body mass index (`BMI`), weight gain (`WtGain`, in pounds), average daily number of cigarettes during pregnancy (`NumCig`), and indicators for the mother receiving sufficient prenatal care (`PreVis`) and having developed pregnancy hypertension (`PHype`). We define receiving sufficient prenatal care as having paid more than 12 prenatal visits (Kriebs, 2010).

All numerical covariates are mapped to the unit interval using min-max normalization. For the response variable `Weight`, we considered min-max normalization, and log transformation followed by min-max normalization. We fit QUINN with $V \in \{15, 25, 30\}$ hidden neurons and $p \in \{10, 15, 20\}$ spline knots. We draw 3500 posterior samples using NUTS, discarding the first 2500 samples as burn-in and choose the best model configuration based on WAIC.

To determine which covariates have significant impact on the birth weight distribution, we first calculate the ALE-induced VI score for each main effect across different quantiles. In particular, we would like to identify the covariates that most impact low birth weight (represented by the 0.05 quantile), typical birth weight (represented by the 0.5 quantile), and high birth weight (represented by the 0.95 quantile). Figure 7 shows the ranking of ALE main effects at $\tau \in \{0.05, 0.50, 0.95\}$. Length of gestation, maternal height, maternal body mass index, weight gain, average daily number

²Source: https://www.cdc.gov/nchs/data_access/vitalstatsonline.htm

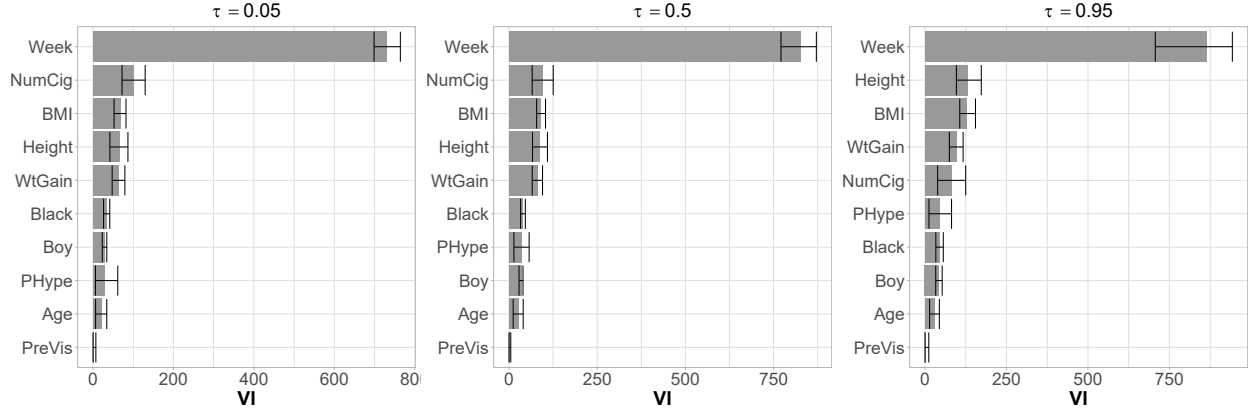
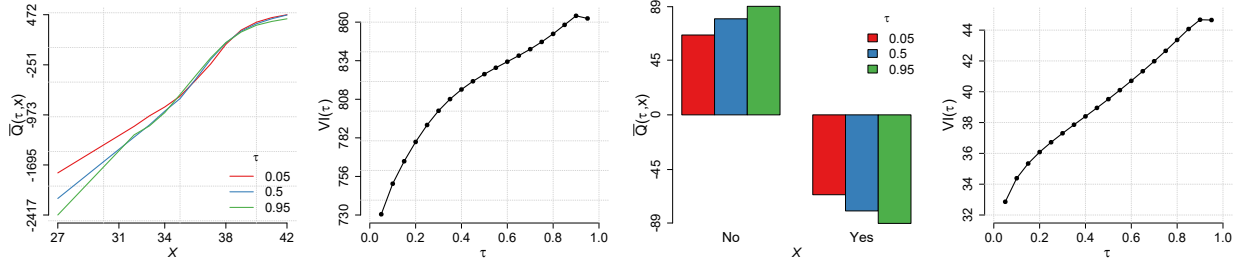


Figure 7: **Marginal main effects importance for the birth weight analysis.** Posterior mean (95% credible interval) of the variable importance $VI_j(\tau)$ of each covariate.

of cigarettes during pregnancy, maternal race, and gender of the newborn are influential on all three quantiles. In particular, length of gestation is the most influential covariate on all three quantiles, average daily number of cigarettes during pregnancy is more influential on low and typical birth weight than on high birth weight, and height is more influential on high birth weight than on low and typical birth weight.

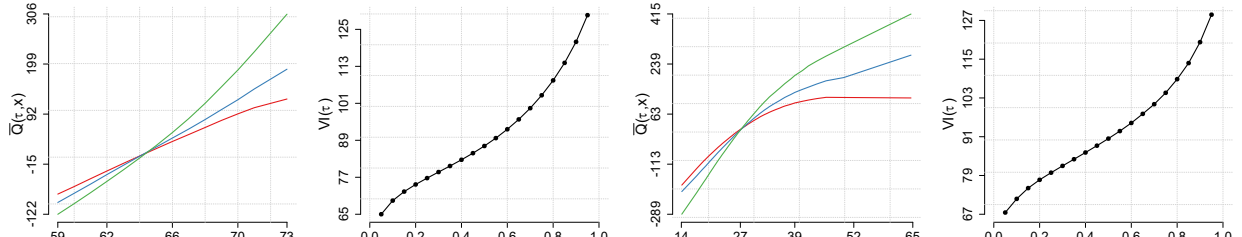
The ALE main effects of the six most important covariates at $\tau \in \{0.05, 0.50, 0.95\}$, as well as their VI over the entire quantile range are plotted in Figure 8. Our results indicate that the influence of these covariates on birth weight are significantly non-constant across quantiles. Longer gestation, increasing maternal height, increasing maternal body mass index, and weight gain contribute to higher birth weight; their effects are more pronounced at the high ends of the weight distribution. Increasing smoking during pregnancy contributes to lower birth weight; its effect is more pronounced at the low ends of the weight distribution. Compared to White mothers, Black mothers are associated with lower birth weight; the difference is most substantial at high ends of the weight distribution.

We further analyze the pair-wise interaction effects between length of gestation, maternal height, maternal body mass index, average daily number of cigarettes during pregnancy, and weight gain. The posterior mean and standard deviation of their variable importance at $\tau \in \{0.05, 0.5, 0.95\}$ are shown in Figure 9. The most important interaction effects all involve the length of gestation. Specifically, length of gestation and average daily number of cigarettes during



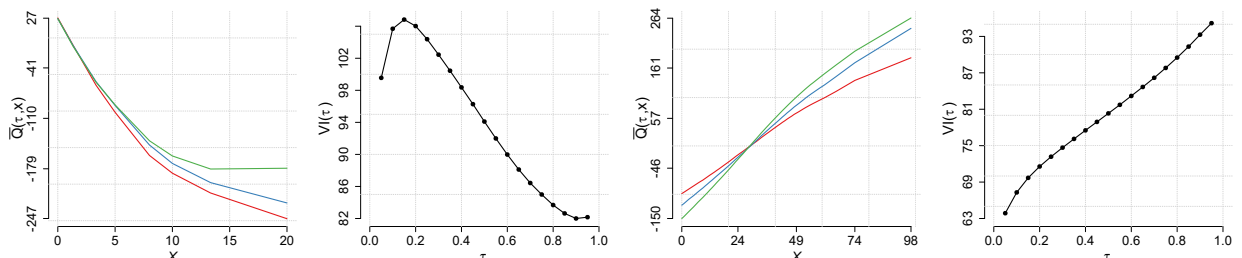
(a) Week

(b) Black



(c) Height

(d) BMI



(e) NumCig

(f) WtGain

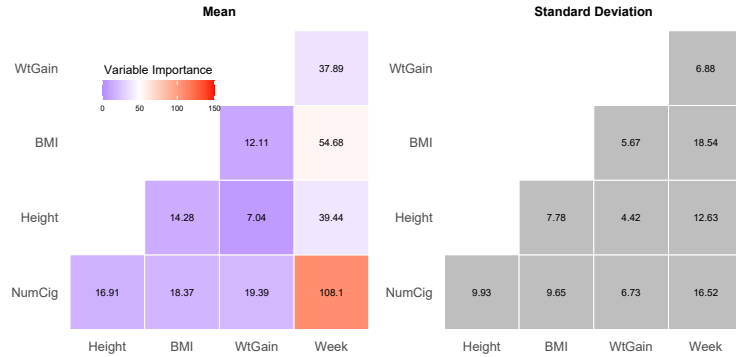
Figure 8: **Marginal main effect estimates for the birth weight analysis.** The plots show the ALE ($\bar{Q}_j(\tau, x_j)$) by quantile level for the six most important covariates.

pregnancy seem to have the most pronounced interaction effect at all three quantiles. A visual illustration of the joint effects of these two covariates at $\tau \in \{0.05, 0.5, 0.95\}$ using contour plots are shown in Figure 10. The results indicate that longer gestation period is associated with higher birth weight irregardless of maternal smoking habit, but the effect is clearly amplified for non-smokers. In addition, heavier maternal smoking is associated with lower birth weight only for infants born after 38 weeks.

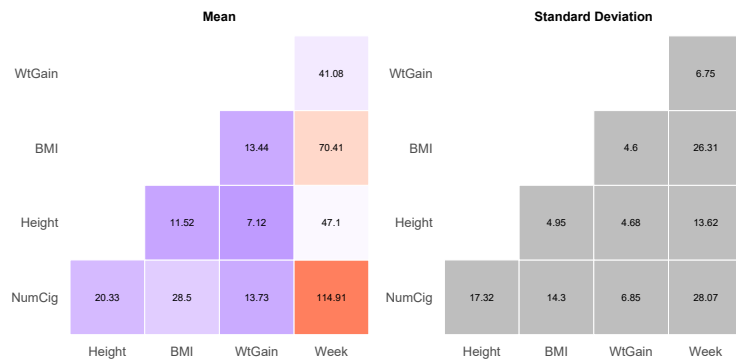
6 Conclusion

In this paper, we propose a novel non-parametric method to simultaneously model non-crossing non-linear quantile curves. The model for the conditional CDF of the response variable uses \mathcal{I} -spline series expansion, where the spline coefficients are further modeled as functions of covariates using FNNs. By leveraging the approximation power of splines and neural networks, our model can approximate all continuous CDFs, and thus all continuous quantile functions. We adopt a Bayesian framework by assigning prior distributions to the weight parameters and utilize the state-of-art NUTS to sample efficiently from the high-dimensional posterior. The performance of our model depends on the number of hidden neurons and spline knots which are selected using WAIC. Compared to existing simultaneous quantile regression methods, our method can estimate the whole quantile process, yields a smooth estimate of the quantile function, and scales to high-dimensional regression. We also show that our model can yield meaningful interpretation via ALE plots and variable importance scores. Simulation studies show that our method can better recover the generating quantile process than existing methods, particularly when the sample size is small; and the relative importance of main and interaction effects can be estimated accurately.

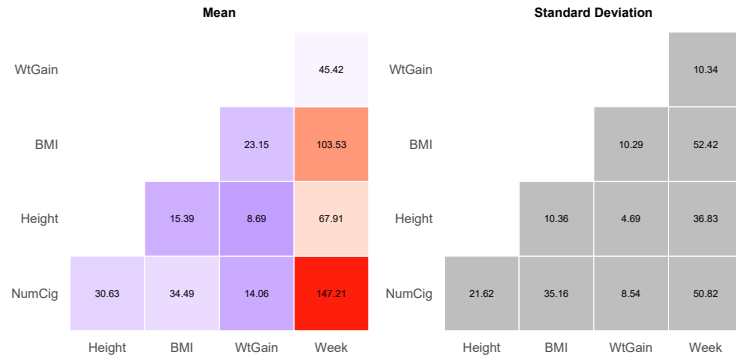
The proposed model was applied to the intensity data of tropical cyclones in the North Atlantic Basin and specifically to investigate how intensity quantiles changed between years 1981 and 2006. Our results showed that cyclone intensity increased smoothly from 1981 to 2006, with intensity of the strongest cyclones increasing more significantly than that of typical and weak cyclones. The proposed method was also used to analyze the relationship between birth weight and maternal characteristics of U.S. newborns and specifically to identify the important maternal characteristics



(a) Quantile level $\tau = 0.05$



(b) Quantile level $\tau = 0.50$



(c) Quantile level $\tau = 0.95$

Figure 9: **Marginal interaction effects importance for the birth weight analysis.** Posterior mean and standard deviation of variable importance $VI_{jk}(\tau)$ for interaction effects between influential covariates.

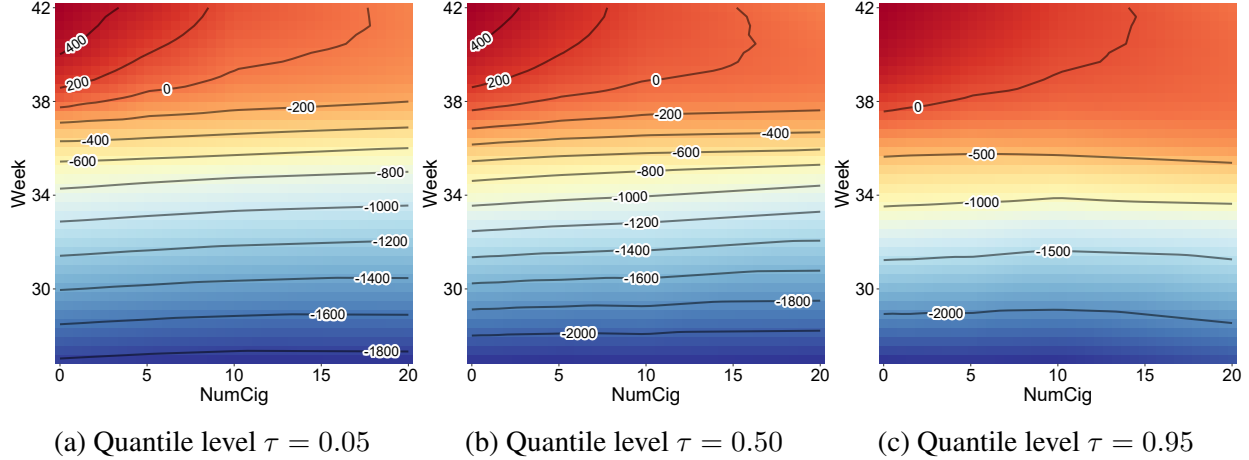


Figure 10: **Marginal interaction effect estimates for the birth weight analysis.** Posterior mean of second-order ALE $\bar{Q}_{jl}(\tau)$ for joint effects of length of gestation (Week) and average daily number of cigarettes (NumCig) at $\tau \in \{0.05, 0.5, 0.95\}$.

that are associated with high and low birth weight. Our results showed that low birth weight is primarily associated with prematurity, heavy maternal smoking, Black mothers; whereas high birth weight is primarily associated high maternal body mass index, maternal height, and maternal weight gain.

A crucial step in fitting our model is a transformation of the original response into the unit interval. In this paper, we found that the min-max normalization sufficed in most cases. However, when the response is unbounded, the min-max normalization truncates the response distribution, potentially impacting estimation accuracy of extreme quantiles of heavy-tailed distributions. For practical use, we recommend different transformation methods to be compared, including those that depend on the covariate vector (e.g. conditional CDF transformation). Our current model assumes independence between observations as well as between covariates. Future work can focus on relaxing these assumptions, such as the accommodation of spatial and/or temporal correlation between observations, and highly correlated covariates.

References

Abrevaya, J. (2001) The effects of demographics and maternal behavior on the distribution of birth outcomes. *Empirical Economics*, **26**, 247–257.

Apley, D. W. and Zhu, J. (2020) Visualizing the effects of predictor variables in black box supervised learning models. *Journal of the Royal Statistical Society: Series B (Statistical Methodology)*, **82**, 1059–1086.

Betancourt, M. (2017) A conceptual introduction to Hamiltonian Monte Carlo. *arXiv preprint arXiv:1701.02434*.

Betancourt, M. and Girolami, M. (2015) Hamiltonian Monte Carlo for hierarchical models. *Current Trends in Bayesian Methodology with Applications*, **79**, 2–4.

Bondell, H. D., Reich, B. J. and Wang, H. (2010) Noncrossing quantile regression curve estimation. *Biometrika*, **97**, 825–838.

Breiman, L. (2001) Random forests. *Machine Learning*, **45**, 5–32.

Cannon, A. J. (2018) Non-crossing nonlinear regression quantiles by monotone composite quantile regression neural network, with application to rainfall extremes. *Stochastic Environmental Research and Risk Assessment*, **32**, 3207–3225.

Chernozhukov, V., Fernández-Val, I. and Galichon, A. (2010) Quantile and probability curves without crossing. *Econometrica*, **78**, 1093–1125.

Das, P. and Ghosal, S. (2018) Bayesian non-parametric simultaneous quantile regression for complete and grid data. *Computational Statistics & Data Analysis*, **127**, 172–186.

De Boor, C. and Daniel, J. W. (1974) Splines with nonnegative \mathcal{B} -spline coefficients. *Mathematics of Computation*, **28**, 565–568.

Elsner, J. B., Kossin, J. P. and Jagger, T. H. (2008) The increasing intensity of the strongest tropical cyclones. *Nature*, **455**, 92–95.

Friedman, J. H. (2001) Greedy function approximation: a gradient boosting machine. *The Annals of Statistics*, 1189–1232.

Geman, S. and Geman, D. (1984) Stochastic relaxation, Gibbs distributions, and the Bayesian restoration of images. *IEEE Transactions on Pattern Analysis and Machine Intelligence*, 721–741.

Goldstein, A., Kapelner, A., Bleich, J. and Pitkin, E. (2015) Peeking inside the black box: Visualizing statistical learning with plots of individual conditional expectation. *Journal of Computational and Graphical Statistics*, **24**, 44–65.

Greenwell, B. M., Boehmke, B. C. and McCarthy, A. J. (2018) A simple and effective model-based variable importance measure. *arXiv preprint arXiv:1805.04755*.

Hoffman, M. D. and Gelman, A. (2014) The No-U-Turn sampler: adaptively setting path lengths in Hamiltonian Monte Carlo. *Journal of Machine Learning Research*, **15**, 1593–1623.

Holmes, M. P., Gray, A. G. and Isbell, C. L. (2012) Fast nonparametric conditional density estimation. *arXiv preprint arXiv:1206.5278*.

Izbicki, R. and Lee, A. B. (2016) Nonparametric conditional density estimation in a high-dimensional regression setting. *Journal of Computational and Graphical Statistics*, **25**, 1297–1316.

Koenker, R. and Bassett Jr, G. (1978) Regression Quantiles. *Econometrica*, 33–50.

Kriebs, J. M. (2010) Guidelines for Perinatal Care, Sixth Edition: By the American Academy of Pediatrics and the American College of Obstetricians and Gynecologists. *Journal of Midwifery & Women's Health*.

Li, R., Bondell, H. D. and Reich, B. J. (2021) Deep distribution regression. *In press, Computational Statistics and Data Analysis*.

Liu, Y. and Wu, Y. (2009) Stepwise multiple quantile regression estimation using non-crossing constraints. *Statistics and Its Interface*, **2**, 299–310.

— (2011) Simultaneous multiple non-crossing quantile regression estimation using kernel constraints. *Journal of Nonparametric Statistics*, **23**, 415–437.

Metropolis, N., Rosenbluth, A. W., Rosenbluth, M. N., Teller, A. H. and Teller, E. (1953) Equation of state calculations by fast computing machines. *The Journal of Chemical Physics*, **21**, 1087–1092.

Monnahan, C. C. and Kristensen, K. (2018) No-U-turn sampling for fast Bayesian inference in ADMB and TMB: Introducing the adnuts and tmbstan R packages. *PLoS ONE*, **13**, e0197954.

Muggeo, V. M., Sciandra, M., Tomasello, A. and Calvo, S. (2013) Estimating growth charts via nonparametric quantile regression: a practical framework with application in ecology. *Environmental and Ecological Statistics*, **20**, 519–531.

Neal, R. M. (2011) MCMC using Hamiltonian dynamics. In *Handbook of Markov Chain Monte Carlo* (eds. S. Brooks, A. Gelman, G. L. Jones and X. L. Meng), chap. 5, 113–162. Chapman & Hall/CRC.

— (2012) *Bayesian learning for neural networks*, vol. 118. Springer Science & Business Media.

Reich, B. J. (2012) Spatiotemporal quantile regression for detecting distributional changes in environmental processes. *Journal of the Royal Statistical Society: Series C (Applied Statistics)*, **61**, 535–553.

Reich, B. J., Fuentes, M. and Dunson, D. B. (2011) Bayesian spatial quantile regression. *Journal of the American Statistical Association*, **106**, 6–20.

Reich, B. J. and Smith, L. B. (2013) Bayesian quantile regression for censored data. *Biometrics*, **69**, 651–660.

Ribeiro, M. T., Singh, S. and Guestrin, C. (2016) Model-agnostic interpretability of machine learning. *arXiv preprint arXiv:1606.05386*.

Rodrigues, T. and Fan, Y. (2017) Regression adjustment for noncrossing Bayesian quantile regression. *Journal of Computational and Graphical Statistics*, **26**, 275–284.

Rothfuss, J., Ferreira, F., Walther, S. and Ulrich, M. (2019) Conditional Density Estimation with Neural Networks: Best Practices and Benchmarks. *arXiv:1903.00954*.

Salvatier, J., Wiecki, T. V. and Fonnesbeck, C. (2016) Probabilistic programming in Python using PyMC3. *PeerJ Computer Science*, **2**, e55.

Stan Development Team (2019) Stan Modeling Language Users Guide and Reference Manual. URL <https://mc-stan.org>.

Tokdar, S. T., Kadane, J. B. et al. (2012) Simultaneous linear quantile regression: a semiparametric Bayesian approach. *Bayesian Analysis*, **7**, 51–72.

Yang, Y. and Tokdar, S. T. (2017) Joint estimation of quantile planes over arbitrary predictor spaces. *Journal of the American Statistical Association*, **112**, 1107–1120.

Yuan, Y., Chen, N. and Zhou, S. (2017) Modeling regression quantile process using monotone B-splines. *Technometrics*, **59**, 338–350.

Appendices

A MCMC sampling details

A.1 Posterior evaluation

The non-parametric model on the conditional PDF of Z given $\mathbf{X} = \mathbf{x}$ is

$$f_Z(z|\mathbf{x}, \mathcal{W}) = \sum_{m=1}^{r+p-1} \theta_m(\mathbf{x}, \mathcal{W}) \mathcal{M}_{m,r}(z|\mathbf{T}) = \sum_{m=1}^{r+p-1} \frac{\exp\{u_m(\mathbf{x}, \mathcal{W})\}}{\sum_{i=1}^{r+p-1} \exp\{u_i(\mathbf{x}, \mathcal{W})\}} \mathcal{M}_{m,r}(z|\mathbf{T}),$$

and the likelihood function is

$$\mathcal{L}(\mathcal{D}|\mathcal{W}) = \prod_{i=1}^n f_Z(z_i, \mathbf{x}_i|\mathcal{W}) = \prod_{i=1}^n \left\{ \sum_{m=1}^{r+p-1} \frac{\exp\{u_m(\mathbf{x}_i, \mathcal{W})\}}{\sum_{j=1}^{r+p-1} \exp\{u_j(\mathbf{x}_i, \mathcal{W})\}} \mathcal{M}_{m,r}(z_i|\mathbf{T}) \right\}.$$

where $\mathcal{D} = \{z_i, \mathbf{x}_i\}_{i=1}^n$ denotes the observed data. Let $\Theta = \{\mathcal{W}, \sigma_w, \gamma\}$ denote the set of modeling parameters and hyper-parameters, then the posterior of QUINN is

$$f(\Theta|\mathcal{D}) \propto \mathcal{N}^+(\gamma|0, a^2) \prod_{m=1}^{r+p-1} \prod_{l=0}^V \mathcal{N}(W_{2ml}|0, \gamma^2) \prod_{j=0}^d \mathcal{N}^+(\sigma_j|0, a^2) \\ \prod_{l=0}^V \prod_{j=0}^d \mathcal{N}(W_{1lj}|0, \sigma_j^2) \prod_{i=1}^n f_Z(z_i, \mathbf{x}_i|\mathcal{W})$$

which can be approximated using MCMC methods. Sampling from this posterior is challenging for traditional MCMC methods such as random-walk Metropolis (Metropolis et al., 1953) and Gibbs sampler (Geman and Geman, 1984). These methods, although straightforward to implement, do not scale well to complicated posterior with high-dimensional parameter space. The former explores the posterior via inefficient random walks, resulting in low acceptance rate and wasted samples; the latter requires knowing the conditional distribution of each parameter, which can be unrealistic in high-dimensional case.

A.2 Hamiltonian Monte Carlo

Hamiltonian Monte Carlo (HMC) (Neal, 2011; Betancourt and Girolami, 2015; Betancourt, 2017) is a variant of MCMC that permits efficient sampling from a high-dimensional target distribution, provided that all model parameters are continuous. It has gained increasing popularity for its recent applications in inference of Bayesian neural networks (Neal, 2012). By introducing auxillary variables \mathbf{r} , HMC transforms the problem of sampling from $f(\Theta|\mathcal{D})$ to sampling from the joint distribution $f(\mathbf{r}, \Theta|\mathcal{D}) = f(\mathbf{r}|\Theta, \mathcal{D})f(\Theta|\mathcal{D})$ where $f(\mathbf{r}|\Theta, \mathcal{D})$ is the auxiliary distribution often assumed to be multivariate Normal and independent of Θ and \mathcal{D} , i.e. $f(\mathbf{r}|\Theta, \mathcal{D}) = f(\mathbf{r})$. The joint

distribution defines a Hamiltonian

$$\begin{aligned} H(\mathbf{r}, \Theta | \mathcal{D}) &= T(\mathbf{r}) + V(\Theta | \mathcal{D}) \\ T(\mathbf{r}) &:= -\log f(\mathbf{r}) \\ V(\Theta | \mathcal{D}) &:= -\log f(\Theta | \mathcal{D}). \end{aligned}$$

which can be used to generate states, i.e. samples of Θ and \mathbf{r} , by simulating the Hamiltonian dynamics

$$\frac{\partial \Theta}{\partial t} = \frac{\partial T}{\partial \mathbf{r}}, \quad \frac{\partial \mathbf{r}}{\partial t} = \frac{\partial V}{\partial \Theta}.$$

At any state (Θ_t, \mathbf{r}_t) , HMC proposes the next state $(\Theta_{t+L\Delta t}, \mathbf{r}_{t+L\Delta t})$ by simulating Hamiltonian dynamics for time $L\Delta t$, which is approximated by applying the leapfrog algorithm L times each with step size Δt . Starting from an initial state, this process is repeated and the visited states form a Markov chain. Compared to random-walk Metropolis, HMC explores the target distribution more efficiently by using gradient of the log-posterior to direct each transition of the Markov chain. Although each step is more computationally expensive than a Metropolis proposal, the Markov chain produced by HMC often yields more distant samples and significantly higher acceptance rate. Although HMC has a high potential, its practical performance depends highly on the values of L and Δt . Poor choice of either parameter will result in unsatisfactory exploration of the posterior. In this paper, instead of using the original HMC which only allows manual setting of L and Δt , we use the No-U-Turn Sampler (NUTS). NUTS is an extension to HMC that implements automatic tuning of L . Furthermore, we use the dual averaging algorithm to adaptively select Δt . A detailed description of NUTS with dual averaging is presented in Algorithm 6 of Hoffman and Gelman (2014).

NUTS is implemented in many probabilistic programming framework, such as PyMC3 (Salvatier et al., 2016) and Stan (Stan Development Team, 2019). Computational complexity of an HMC implementation is contingent on gradient calculation of the log-posterior, which the aforementioned high-level frameworks handle via automatic differentiation. In our experiment, we observe that automatic differentiation can be extremely time consuming for a posterior as high-dimensional as ours. As a result, we use a low-level R implementation (Monnahan and Kristensen,

2018) that accepts analytic gradients which we manually calculate.

A.3 Reparametrization and transformation

The hierarchical Gaussian priors $W_{1vw} \stackrel{\text{indep}}{\sim} \mathcal{N}(0, \sigma_w^2)$, $\sigma_w \stackrel{iid}{\sim} \mathcal{N}^+(0, a^2)$ introduce strong correlation between W_{1vw} and σ_w in the posterior, especially when the data size is small. To alleviate this issue, we consider a reparametrization:

$$B_{1vw} \stackrel{iid}{\sim} \mathcal{N}(0, 1), \sigma_w \stackrel{iid}{\sim} \mathcal{N}^+(0, a^2), W_{1vw} = \sigma_w B_{1vw}$$

where B_{1vw} can be considered as standardized weights. Because B_{1vw} and σ_w follow independent prior distributions, they are marginally uncorrelated in the posterior. Their coupling is instead introduced in the likelihood function. Such a parameterization is called non-centered. Non-centered parameterization leads to simpler posterior geometries, thus increasing the efficiency of HMC. Similarly, $W_{2vw} \stackrel{\text{indep}}{\sim} \mathcal{N}(0, \gamma^2)$, $\gamma \sim \mathcal{N}^+(0, a^2)$ can be reparameterized as

$$B_{2vw} \stackrel{iid}{\sim} \mathcal{N}(0, 1), \gamma \sim \mathcal{N}^+(0, a^2), W_{2vw} = \gamma B_{2vw}.$$

HMC requires Θ to lie in an unconstrained space, and thus every parameter that has a natural constraint needs to be transformed to an unconstrained variable. After unconstrained posterior samples are drawn, they can be back-transformed to the constrained space. In Θ , the scale parameters σ_v and γ are naturally constrained to be positive. Therefore we work with their log-transformations $\tilde{\sigma}_v = \log \sigma_v$ and $\tilde{\gamma} = \log \gamma$ with transformed prior distributions

$$f(\tilde{\sigma}_v) = \mathcal{N}^+(\exp(\tilde{\sigma}_v)|0, a^2) \exp(\tilde{\sigma}_v) \quad \text{and} \quad f(\tilde{\gamma}) = \mathcal{N}^+(\exp(\tilde{\gamma})|0, a^2) \exp(\tilde{\gamma}).$$

Let $\mathcal{B} = \{\beta_{uvw}\}$ and $\tilde{\Theta} = \{\mathcal{B}, \tilde{\sigma}_w, \tilde{\gamma}\}$, then the posterior after non-centered reparameterization

and constraint transformation is

$$f(\tilde{\Theta}|\mathcal{D}) \propto \mathcal{N}^+(\exp(\tilde{\gamma})|0, a^2) \exp(\tilde{\gamma}) \prod_{m=1}^{r+p-1} \prod_{l=0}^V \mathcal{N}(B_{2ml}|0, 1) \prod_{j=0}^d \mathcal{N}^+(\exp(\tilde{\sigma})_j|0, a^2) \exp(\tilde{\sigma}_j) \\ \prod_{l=0}^V \prod_{j=0}^d \mathcal{N}(B_{1lj}|0, 1) \prod_{i=1}^n f_Z(z_i, \mathbf{x}_i|\mathcal{W}),$$

where $W_{1vw} = \exp(\tilde{\sigma}_w)B_{1vw}$ and $W_{2vw} = \exp(\tilde{\gamma})B_{2vw}$ in the likelihood function.

A.4 Analytic gradient

In this section, we provide analytic formulas for computing the gradient of $\log f(\tilde{\Theta}|\mathcal{D})$, which NUTS uses to generate samples of $\tilde{\Theta}$. To start with, let \mathbf{X} denote the observed covariate matrix, $\mathbf{M}_r(\mathbf{z}|\mathbf{T})$ denote the \mathcal{M} -spline matrix of transformed response vector \mathbf{z} , $\mathbf{1}$ denote a column vector of 1s, $\boldsymbol{\sigma}$ denote the vector with elements σ_w , and \mathbf{B}_u denote the matrix with elements B_{uvw} . The log-likelihood function parametrized by $\tilde{\Theta}$ can be written in a compact form

$$\ell(\mathcal{D}|\tilde{\Theta}) = \sum_{i=1}^n \left(\log \left[\sum_{m=1}^{r+p-1} \exp \left\{ u_m(\mathbf{x}_i, \tilde{\Theta}) \right\} \mathcal{M}_{m,r}(z_i|\mathbf{T}) \right] - \log \left[\sum_{m=1}^{r+p-1} \exp \left\{ u_m(\mathbf{x}_i, \tilde{\Theta}) \right\} \right] \right) \\ = \mathbf{1}^T \left(\log \left[\exp \left\{ \mathbf{U}(\mathbf{X}, \tilde{\Theta}) \right\} \odot \mathbf{M}_r(\mathbf{z}|\mathbf{T}) \mathbf{1} \right] - \log \left[\exp \left\{ \mathbf{U}(\mathbf{X}, \tilde{\Theta}) \right\} \mathbf{1} \right] \right)$$

where

$$\mathbf{U}(\mathbf{X}, \tilde{\Theta}) = \left(\mathbf{1} \mid \phi \left\{ \tilde{\mathbf{X}} \text{diag}[\exp(\tilde{\boldsymbol{\sigma}})] \mathbf{B}_1 \right\} \right) [\exp(\tilde{\gamma}) \mathbf{B}_2], \quad \tilde{\mathbf{X}} = \left(\mathbf{1} \mid \mathbf{X} \right),$$

and $\text{diag}[\exp(\tilde{\boldsymbol{\sigma}})]$ is the diagonal matrix with diagonal entries $\exp(\tilde{\boldsymbol{\sigma}})$. The log-prior can be written as

$$f(\tilde{\Theta}) \propto -\frac{\exp(2\tilde{\gamma})a^2}{\pi} + \tilde{\gamma} - \frac{\text{vec}(\mathbf{B}_2)^T \text{vec}(\mathbf{B}_2)}{2} - \mathbf{1}^T \left[\frac{\exp(2\tilde{\boldsymbol{\sigma}})a^2}{\pi} - \tilde{\boldsymbol{\sigma}} \right] - \frac{\text{vec}(\mathbf{B}_1)^T \text{vec}(\mathbf{B}_1)}{2}.$$

where $\text{vec}(\cdot)$ denotes the vectorization operator. Finally, the gradient formula of the log-posterior with respect to each parameter is given by

$$\begin{aligned}
\frac{\partial \log f(\tilde{\Theta}|\mathcal{D})}{\partial \mathbf{B}_1} &= \exp(\tilde{\gamma}) \text{diag}[\exp(\tilde{\sigma})] \tilde{\mathbf{X}}^T (\mathbf{V}_1 \mathbf{V}_3 - \mathbf{V}_2 \mathbf{V}_3) - \mathbf{B}_1 \\
\frac{\partial \log f(\tilde{\Theta}|\mathcal{D})}{\partial \mathbf{B}_2} &= \exp(\tilde{\gamma}) \mathbf{V}_0^T \left(\mathbf{V}_1 \left[\exp \left\{ \mathbf{U}(\mathbf{X}, \tilde{\Theta}) \right\} \odot \mathbf{M}_r(\mathbf{z}|\mathbf{T}) \right] - \mathbf{V}_2 \exp \left\{ \mathbf{U}(\mathbf{X}, \tilde{\Theta}) \right\} \right) - \mathbf{B}_2 \\
\frac{\partial \log f(\tilde{\Theta}|\mathcal{D})}{\partial \tilde{\sigma}} &= \exp(\tilde{\gamma}) \left[\text{diag} \left\{ \tilde{\mathbf{X}}^T (\mathbf{V}_1 \mathbf{V}_3 - \mathbf{V}_2 \mathbf{V}_4) \mathbf{B}_1^T \right\} \right] \odot \exp(\tilde{\sigma}) - \frac{2a^2}{\pi} \exp(2\tilde{\sigma}) + 1 \\
\frac{\partial \log f(\tilde{\Theta}|\mathcal{D})}{\partial \tilde{\gamma}} &= \exp(\tilde{\gamma}) \left(\text{tr} \left\{ \mathbf{V}_0 \mathbf{B}_2 \left[\exp \left\{ \mathbf{U}(\mathbf{X}, \tilde{\Theta}) \right\} \odot \mathbf{M}_r(\mathbf{z}|\mathbf{T}) \right]^T \mathbf{V}_1 \right\} \right. \\
&\quad \left. - \text{tr} \left\{ \mathbf{V}_0 \mathbf{B}_2 \exp \left\{ \mathbf{U}(\mathbf{X}, \tilde{\Theta}) \right\}^T \mathbf{V}_2 \right\} \right) - \frac{2a^2}{\pi} \exp(2\tilde{\gamma}) + 1
\end{aligned}$$

where

$$\begin{aligned}
\mathbf{V}_0 &= \left(\mathbf{1} \mid \phi \left\{ \tilde{\mathbf{X}} \text{diag}[\exp(\tilde{\sigma})] \mathbf{B}_1 \right\} \right) \\
\mathbf{V}_1 &= \text{diag} \left\{ \mathbf{1} \oslash \left[\exp \left\{ \mathbf{U}(\mathbf{X}, \tilde{\Theta}) \right\} \odot \mathbf{M}_r(\mathbf{z}|\mathbf{T}) \mathbf{1} \right] \right\} \\
\mathbf{V}_2 &= \text{diag} \left\{ \mathbf{1} \oslash \left[\exp \left\{ \mathbf{U}(\mathbf{X}, \tilde{\Theta}) \right\} \mathbf{1} \right] \right\} \\
\mathbf{V}_3 &= \left[\exp \left\{ \mathbf{U}(\mathbf{X}, \tilde{\Theta}) \right\} \odot \mathbf{M}_r(\mathbf{z}|\mathbf{T}) \bar{\mathbf{B}}_2^T \right] \odot \phi' \left(\tilde{\mathbf{X}} \text{diag}[\exp(\tilde{\sigma})] \mathbf{B}_1 \right) \\
\mathbf{V}_4 &= \left[\exp \left\{ \mathbf{U}(\mathbf{X}, \tilde{\Theta}) \right\} \bar{\mathbf{B}}_2^T \right] \odot \phi' \left(\tilde{\mathbf{X}} \text{diag}[\exp(\tilde{\sigma})] \mathbf{B}_1 \right),
\end{aligned}$$

\odot denotes element-wise multiplication, \oslash denotes element-wise division, and $\bar{\mathbf{B}}_u$ is \mathbf{B}_u after removing the first row.

A.5 Model estimation

It is well-known that FNN suffers from over-parameterization, which makes the weight parameters highly non-identifiable. In practice, MCMC for individual weights might not even converge, making Bayesian inference of the weight parameters impossible. Let $\mathcal{W}^{(t)}, t = 1, \dots, T$ denote the t th posterior sample of \mathcal{W} . In this study, instead of using the posterior estimates (e.g. posterior

means) of the weight parameters to calculate a single estimate of $F_Z(z|\mathbf{x}, \hat{\mathcal{W}})$

$$\hat{\mathcal{W}} = \frac{1}{T} \sum_{t=1}^T \mathcal{W}^{(t)}$$

we estimate $F_Z(z|\mathbf{x})$ using its posterior mean

$$\hat{F}_Z(z|\mathbf{x}) = \frac{1}{T} \sum_{t=1}^T F(z|\mathbf{x}, \mathcal{W}^{(t)}).$$

Convergence of MCMC can be checked using the trace plot of $F_Z(z|\mathbf{x}, \mathcal{W}^{(t)})$ for some (z, \mathbf{x}) .

B Computing the sensitivity indices

In this section, we first briefly summarize how the main and interaction ALE can be estimated using sample data; the full description can be seen in Apley and Zhu (2020). We then explain how VI scores can be estimate based on the ALE estimates.

Let $x_{i,j}$ and $\mathbf{x}_{i,\setminus j}$ denote the i th observation of j th covariate and all other covariates respectively. The sample range of X_j is partitioned into K intervals $\{N_j(k) = (z_{k-1,j}, z_{k,j}] : k = 1, 2, \dots, K\}$ where $z_{k,j}$ are chosen as the k/K -th sample percentile if X_j is continuous and the unique values otherwise. Then the uncentered effect $\bar{Q}_j^U(\tau, x_j)$ can be estimated by

$$\hat{Q}_j^U(\tau, x_j) = \sum_{k=1}^{k_j(x_j)} \frac{1}{n_j(k)} \sum_{\{i: x_{i,j} \in N_j(k)\}} [q_j(\tau, z_{k,j}, \mathbf{x}_{i,\setminus j}) - q_j(\tau, z_{k-1,j}, \mathbf{x}_{i,\setminus j})],$$

where $k_j(x_j)$ index the interval into which x_j falls, and $n_j(k)$ denotes the number of sample observations $N_j(k)$ contains such that $n = \sum_{k=1}^K n_j(k)$. Finally, $\bar{Q}_j(\tau, x_j)$ can be estimated by mean-centering $\hat{Q}_j^U(\tau, x_j)$, i.e.

$$\hat{Q}_j(\tau, x_j) = \hat{Q}_j^U(\tau, x_j) - \frac{1}{n} \sum_{k=1}^K n_j(k) \bar{Q}_j^U(\tau, z_{k,j}).$$

For any pair of covariates $\{X_j, X_l\}$, let $\mathbf{x}_{i,\{j,l\}}$ denote i th observation vector of j th and l th covariate, and $\mathbf{x}_{i,\setminus\{j,l\}}$ denote all other covariates. The Cartesian product of sample ranges of X_j and X_l can be partitioned into K^2 rectangular cells $N_{\{j,l\}}(k, m) = (z_{k-1,j}, z_{k,j}] \times (z_{l-1,j}, z_{l,j}]$. Then the uncentered effect $\bar{Q}_{jl}^U(\tau, x_j, x_l)$ can be estimated by

$$\begin{aligned}\hat{Q}_{jl}^U(\tau, x_j, x_l) = & \sum_{k=1}^{k_j(x_j)} \sum_{m=1}^{k_l(x_l)} \frac{1}{n_{\{j,l\}}(k, m)} \sum_{\{i: \mathbf{x}_{i,\{j,l\}} \in N_{\{j,l\}}(k, m)\}} \left[q_{jl}(\tau, z_{k,j}, z_{m,l}, \mathbf{x}_{i,\setminus\{j,l\}}) \right. \\ & - q_{jl}(\tau, z_{k-1,j}, z_{m,l}, \mathbf{x}_{i,\setminus\{j,l\}}) - \left\{ q_{jl}(\tau, z_{k,j}, z_{m-1,l}, \mathbf{x}_{i,\setminus\{j,l\}}) \right. \\ & \left. \left. - q_{jl}(\tau, z_{k-1,j}, z_{m-1,l}, \mathbf{x}_{i,\setminus\{j,l\}}) \right\} \right],\end{aligned}$$

where $k_j(x_j), k_l(x_l)$ index the cell into which (x_j, x_l) falls, and $n_{\{j,l\}}(k, m)$ denotes the number of sample observations $N_{\{j,l\}}(k, m)$ contains such that $n = \sum_{k=1}^K \sum_{m=1}^K n_{\{j,l\}}(k, m)$. Similarly, $\bar{Q}_{jl}(\tau, x_j, x_l)$ can be estimated by mean-centering $\hat{Q}_{jl}^U(\tau, x_j, x_l)$, i.e.,

$$\hat{Q}_{jl}(\tau, x_j, x_l) = \hat{Q}_{jl}^U(\tau, x_j, x_l) - \frac{1}{n} \sum_{k=1}^K \sum_{m=1}^K n_{\{j,l\}}(k, m) \hat{Q}_{jl}^U(\tau, z_{k,j}, z_{m,l}).$$

Finally, interaction ALE is estimated by $\hat{Q}_{jl}^I(\tau, x_j, x_l) = \hat{Q}_{jl}(\tau, x_j, x_l) - \hat{Q}_j(\tau, x_l) - \hat{Q}_j(\tau, x_l)$.

Following its definition in Section 3, $\text{VI}_j(\tau)$ can be estimated by the sample standard deviation or the sample range of $\hat{Q}_j(\tau, z_{k,j})$, i.e.,

$$\widehat{\text{VI}}_j(\tau) = \begin{cases} \sqrt{\frac{1}{K} \sum_{k=1}^K \left[\hat{Q}_j(\tau, z_{k,j}) - \frac{1}{K} \sum_{k=1}^K \hat{Q}_j(\tau, z_{k,j}) \right]^2} & \text{if } X_j \text{ is continuous} \\ \left\{ \max_k \left[\hat{Q}_j(\tau, z_{k,j}) \right] - \min_k \left[\hat{Q}_j(\tau, z_{k,j}) \right] \right\} / 4 & \text{if } X_j \text{ is categorical} \end{cases}.$$

By analogy, $\text{VI}_{jl}(\tau)$ can be estimated by the sample standard deviation or the sample range of $\hat{Q}_{jl}^I(\tau, z_{k,j}, z_{m,l})$.

C Simulation study implementation details

For QUINN, we first transform the response variable into unit interval using min-max normalization. The conditional CDF of the transformed response is expanded with second-degree \mathcal{L} -spline (i.e., $r = 2$) with p equidistant knots $\mathbf{T} = \{t_0, t_1, \dots, t_p | t_i = i/p, i = 0, \dots, p\}$. The FNN has single hidden layer and V hidden neurons. We consider $V \in \{5, 8, 10, 15\}$ and $p \in \{5, 8, 10, 12\}$, and select the best configuration of V and p based on WAIC. The scale parameter a of the Half-Gaussian hyperprior for the weights is set to 30 to ensure a weakly informative prior. For MCQRNN, we consider neural networks with a single hidden layer, $V \in \{3, 5, 8, 10, 15\}$ hidden neurons, and weight penalty coefficients $\lambda \in \{e^{-2}, e^{-3}, \dots, e^{-6}\}$. We select the best configuration of V and λ using 5-fold cross-validation. For NPSQR and NPDFSQR, we follow the guidelines provided by Das and Ghosal (2018) and first transform the response variable and covariate(s) into unit intervals using min-max normalization. The response variable and covariate(s) are then expanded using quadratic \mathcal{B} -splines with same number of equidistant knots, denoted as p_{DG} . We fit NPSQR with $p_{\text{DG}} \in \{3, 4, \dots, 10\}$ and NPDFSQR with $p_{\text{DG}} \in \{5, 6, \dots, 10\}$. The optimal p_{DG} for either model is chosen based on the AIC in which maximum likelihood estimates are replaced by posterior means. SeriesCDE contains four tuning parameters: the number of components of the series expansion in the Y direction N_Y , the number of components of the series expansion in the \mathbf{X} direction N_X , the bandwidth parameter ϵ of the Gaussian kernel for constructing the Gram matrix of \mathbf{X} , and the smoothness parameter δ that controls the bumpiness of the estimated conditional density function. The tuning grids are set as $N_X, N_Y \in \{1, 2, \dots, n\}$, $\epsilon \in \{e^{-7}, e^{-6.5}, \dots, e^3\}$, and $\delta \in \{0, 0.05, \dots, 0.5\}$. Following the guidelines provided by Izbicki and Lee (2016), we first select the best configuration of N_X , N_Y , and ϵ using 5-fold cross-validation. We then tune δ using again 5-fold cross-validation by fixing N_X , N_Y , and ϵ at their optimal values.

Since QUINN, NPDFSQR, and seriesCDE all model the distribution function, their results have to be converted to estimates of the quantile function. For QUINN and NPDFSQR, once we obtain the non-parametric CDF estimate of the transformed response $\hat{F}_Z(z|\mathbf{x})$, we evaluate it at 101 equidistant grid-points on the unit interval for each \mathbf{x} . The conditional quantile function $Q_Z(\tau|\mathbf{x})$, $\tau \in (0, 1)$ can then be estimated by interpolation using $\left\{ \hat{F}_Z(z_i, \mathbf{x}) \right\}_{i=1}^{101}$ as input values and the

aforementioned 101 equidistant grid-points as functional output values. Finally, the quantile function of the original response $Q_Y(\tau|\mathbf{x})$ can be estimated by reverting the min-max normalization. For seriesCDE, we first convert the non-parametric density function estimate $\hat{f}_Y(y|\mathbf{x})$ to $\hat{F}_Y(y|\mathbf{x})$ using numerical integration (e.g. trapezoidal rule). We then estimate $Q_Y(\tau|\mathbf{x})$ using the aforementioned interpolation approach.

The above parameters are used for Designs 1-3, but for the multivariate Design 4 we have slightly different tuning parameters. For QUINN, we consider $V \in \{15, 25, 30\}$ and $p \in \{10, 15, 20\}$, and choose the best configuration of V and p based on WAIC; values for all other parameters are same as in Designs 1-3. For MCQRNN, we consider neural networks with either a single or two hidden layers, $V \in \{3, 5, 8, 10, 15\}$ hidden neurons for each hidden layer, and weight penalty coefficients $\lambda \in \{e^{-2}, e^{-3}, \dots, e^{-7}\}$. The best configuration of number of layers, V , and λ are selected using 5-fold cross-validation. We do not consider neural networks with more than two hidden layers as they are not currently implemented in `qrnn`. For seriesCDE, all settings are the same as in Designs 1-3.